HHS Public Access

Author manuscript

Neuron. Author manuscript; available in PMC 2021 March 18.

Published in final edited form as:

Neuron. 2020 March 18; 105(6): 1036–1047.e5. doi:10.1016/j.neuron.2019.12.026.

Dopamine-Evoked Synaptic Regulation in the Nucleus Accumbens Requires Astrocyte Activity

Michelle Corkrum[1,6], **Ana Covelo**[1,2,3,6], **Justin Lines**[1], **Luigi Bellocchio**[2,3], **Marc Pisansky**[1], **Kelvin Loke**[1], **Ruth Quintana**[1], **Patrick E. Rothwell**[1], **Rafael Lujan**[4], **Giovanni Marsicano**[2,3], **Eduardo D. Martin**[5], **Mark J. Thomas**[1], **Paulo Kofuji**[1], **Alfonso Araque**[1,7,*]

[1]Department of Neuroscience, University of Minnesota, Minneapolis, MN 55455, USA

[2]INSERM, U1215 NeuroCentre Magendie, Bordeaux Cedex 33077, France

[3]University of Bordeaux, Bordeaux 33000, France

[4]Instituto de Investigación en Discapacidades Neurológicas (IDINE), Universidad Castilla-La Mancha, Albacete 02008, Spain

[5]Instituto Cajal, CSIC, Madrid 28002, Spain

[6]These authors contributed equally

[7]Lead Contact

SUMMARY

Dopamine is involved in physiological processes like learning and memory, motor control and reward, and pathological conditions such as Parkinson's disease and addiction. In contrast to the extensive studies on neurons, astrocyte involvement in dopaminergic signaling remains largely unknown. Using transgenic mice, optogenetics, and pharmacogenetics, we studied the role of astrocytes on the dopaminergic system. We show that in freely behaving mice, astrocytes in the nucleus accumbens (NAc), a key reward center in the brain, respond with Ca^{2+} elevations to synaptically released dopamine, a phenomenon enhanced by amphetamine. In brain slices, synaptically released dopamine increases astrocyte Ca^{2+}, stimulates ATP/adenosine release, and depresses excitatory synaptic transmission through activation of presynaptic A_1 receptors. Amphetamine depresses neurotransmission through stimulation of astrocytes and the consequent A_1 receptor activation. Furthermore, astrocytes modulate the acute behavioral psychomotor effects of amphetamine. Therefore, astrocytes mediate the dopamine- and amphetamine-induced synaptic regulation, revealing a novel cellular pathway in the brain reward system.

*Correspondence: araque@umn.edu.

AUTHOR CONTRIBUTIONS

M.C. and A.C. performed the experiments and analyzed the data. J.L. created custom MATLAB script for fiber photometry data analysis. M.P. and P.R. contributed expertise for fiber photometry experiments. J.L., L.B., and G.M. contributed to behavior experiments. E.D.M contributed expertise for *in vivo* experiments. R.Q. and P.K. performed immunohistochemistry. K.L. conducted stereotaxic surgeries. R.L. performed electron microscopy. M.J.T. aided in planning and interpreting experiments. M.C., A.C., and A.A. conceived the study and wrote the manuscript. All the authors read and edited the manuscript.

DECLARATION OF INTERESTS

The authors declare no competing financial interests.

SUPPLEMENTAL INFORMATION

Supplemental Information can be found online at https://doi.org/10.1016/j.neuron.2019.12.026.

In Brief

Corkrum et al. report that astrocyte activity is required for dopamine- and amphetamine-evoked synaptic regulation and amphetamine-induced locomotor effects. Their study reveals astrocytes as active components of dopaminergic signaling and the brain reward system.

INTRODUCTION

Dopaminergic signaling plays fundamental roles in both physiologic and pathologic brain states. Dopamine is essential for movement, reward, learning, and memory, and it is implicated in brain disorders such as Parkinson's disease and drug addiction. The nucleus accumbens (NAc) is a key brain region in reward and addiction that receives extensive dopaminergic input from the ventral tegmental area (VTA) (Lüscher, 2016; Lüscher and Malenka, 2011). Dopamine depresses glutamatergic neurotransmission in the NAc (Bamford et al., 2008; Kalivas and Volkow, 2005) but the underlying mechanism remains unclear. While some reports indicate that dopamine acts on presynaptic D_1 receptors to directly depress excitatory transmission (Harvey and Lacey, 1996; Nicola et al., 1996), adenosine signaling has also been implicated in dopamine-evoked excitatory depression (Harvey and Lacey, 1997; Kombian et al., 2003; Wang et al., 2012). In contrast to the extensive studies on the function of neurons in dopaminergic signaling in the NAc, the effects of dopamine on astrocyte activity and the consequences on neurotransmission are largely unknown.

Astrocytes have traditionally been considered support cells of the brain aiding in ion homeostasis, maintaining the blood-brain barrier, and providing trophic support to neurons. Accumulating data show that astrocytes also play active roles in brain physiology, being key players in the tripartite synapse (Araque et al., 1999). Astrocytes exhibit increases in intracellular Ca^{2+} in response to neurotransmitters (Araque et al., 2001, 2014; Di Castro et al., 2011; Haydon and Carmignoto, 2006; Navarrete and Araque, 2010; Panatier et al., 2011; Perea et al., 2009, 2016; Volterra et al., 2014; Volterra and Meldolesi, 2005) and, in turn, they release neuroactive substances termed gliotransmitters (Volterra and Meldolesi, 2005) that regulate synaptic transmission and plasticity (Araque et al., 2014; Bezzi et al., 2004; Covelo and Araque, 2016, 2018; Di Castro et al., 2011; Halassa and Haydon, 2010; Henneberger et al., 2010; Martin-Fernandez et al., 2017; Martín et al., 2015; Min and Nevian, 2012; Min et al., 2012; Navarrete and Araque, 2010; Panatier et al., 2011; Parri et al., 2001; Perea and Araque, 2007; Perea et al., 2016; Volterra and Meldolesi, 2005). The bidirectional signaling between neurons and astrocytes has been shown in many brain areas (Araque et al., 2014); however, the specific role of astrocytes in NAc dopamine signaling remains unknown.

Here we show that opto-stimulation of dopaminergic axons in freely moving animals evokes Ca^{2+} elevations in NAc astrocytes and that these responses are altered by amphetamine. Using brain slices to identify the cellular signaling and physiological consequences, we show that astrocyte Ca^{2+} elevations evoked by synaptically released dopamine stimulate the release of ATP/adenosine, which mediates dopamine- and amphetamine-evoked depression of excitatory transmission through activation of A_1 receptors. We also found that selective pharmacogenetic activation of astrocytes mimics the dopamine-evoked synaptic regulation.

Additionally, attenuation of astrocyte Ca^{2+} signaling decreases the acute psychomotor behavioral effects of amphetamine, indicating that astrocytes are actively involved in the dopaminergic system.

RESULTS

Dopamine Activates Astrocyte Ca^{2+} Signaling in the NAc

Astrocytes in the globus pallidus and hippocampus (Cui et al., 2016; Jennings et al., 2017) have been shown to respond to dopamine, but whether astrocytes respond *in vivo* to synaptically released dopamine in reward centers such as the NAc remains unknown. We monitored astrocyte Ca^{2+} levels in the NAc using a fiber-photometry system in freely behaving mice (Lerner et al., 2015; Saunders et al., 2018) and specifically stimulated dopaminergic afferents to the NAc using optogenetics (Figures 1A and 1B). Mice expressing Cre under the dopamine transporter (DAT) promoter (DAT-IRES-Cre mice) were injected with AAV5-hSyn-FLEX-ChrimsonR-tdTomato into the VTA to selectively express ChrimsonR (a red-shifted channelrhodopsin; Klapoetke et al., 2014) in dopaminergic neurons projecting to the NAc (Figure 1A and Figures S1A and S1B). Mice were also injected in the NAc with AAV5-GfaABC1D-cytoGCaMP6f-SV40 to express the Ca^{2+} indicator GCaMP6f selectively in astrocytes (Figure 1A and Figure S2C). Opto-stimulation of dopaminergic axons (5 ms pulses for 5 s) reliably evoked Ca^{2+} elevations in NAc astrocytes in a frequency-dependent manner (Figure 1C). These responses were absent in DAT-Cre mice injected with AAV5-GfaABC1D-GFP (i.e., an injection lacking GCamp6f) in the NAc and in DAT-Cre WT (Cre-negative mice) injected with hSyn-FLEX-ChrimsonR-TdTomato in the VTA (Figure 1D), indicating that they were not artifacts due to opto-stimulation, and they were abolished by flupenthixol (5 mg/kg), confirming that the recorded signal was evoked by dopamine (Figure 1D). Moreover, the amplitude, rise time, and width of the dopamine-evoked astrocyte Ca^{2+} responses were augmented by amphetamine (2.5 mg/kg) (n = 19 responses in control and n = 19 responses in amphetamine from n = 5 animals; Figures 1E and 1F), which is consistent with its known mode of action to increase synaptic dopamine (Calipari and Ferris, 2013). Taken together, these *in vivo* results indicate that NAc astrocytes respond with Ca^{2+} elevations to dopamine released by synaptic terminals from the VTA, and that these responses are regulated by amphetamine.

Ultrastructural results from electron microscopy experiments indicate that D_1 receptors localize not only at the axon terminals and in the postsynaptic terminals, but also in astrocytes (Figure 1G), suggesting that astrocytes are able to sense dopamine and that the recorded responses could result from direct activation of astrocytes by dopamine.

To test this idea, we used brain slices to examine astrocyte responsiveness to dopamine. Local application of dopamine from a micropipette (500 μM, 5 s, 0.5 bar) in the presence of TTX (1 μM) elevated Ca^{2+} in 47 out of 75 astrocytes (n = 7). Dopamine stimulation of astrocytes, manifested as increased Ca^{2+} activity, quantified as Ca^{2+} event probability (Covelo and Araque, 2018; Gómez-Gonzalo et al., 2015; Martin-Fernandez et al., 2017; Martín et al., 2015; Navarrete and Araque, 2010; Perea et al., 2016), occurred in both somas (from 0.14 ± 0.05 to 0.63 ± 0.07, n = 7 slices, Figures 2A and 2B) and processes (from 0.19 ± 0.04 to 0.54 ± 0.07, n = 7 slices, Figures 2A and 2B). Astrocyte responsiveness to

dopamine remained in the presence of a cocktail of neurotransmitter receptor antagonists (CNQX [20 μM], AP5 [50 μM], MPEP [50 μM], LY367385 [100 μM], picrotoxin [50 μM], CGP5462 [1 μM], atropine [50 μM], CPT [10 μM], and suramin [100 μM]) that also contained TTX (1 μM; Figure 2B), suggesting that dopamine acts on NAc astrocytes to elevate Ca^{2+} levels. While these results suggest that the dopamine-evoked Ca^{2+} responses were mediated by direct activation of astrocytes, an indirect effect mediated by a neuronal signal cannot be totally ruled out. However, a more specific approach of deleting D1 receptors only in astrocytes using the GFAP-$D_1^{-/-}$ mice further indicates that dopamine-evoked Ca^{2+} responses were mediated by direct activation of astrocytic D_1 receptors (see below, Figures 4C and 4D). We then investigated astrocyte responsiveness to synaptically released dopamine using the optogenetic approach described above in the presence of the cocktail of neurotransmitter receptor antagonists without TTX. Opto-stimulation of dopaminergic axons (5 ms pulses for 5 s at 30 Hz) elevated astrocyte Ca^{2+} in 39 out of 110 astrocytes, in both somas (from 0.11 ± 0.04 to 0.37 ± 0.06, n = 14 slices) and processes (from 0.19 ± 0.03 to 0.40 ± 0.03, n = 6 slices) in mice expressing ChrimsonR (Figures 2C and 2D), but not in control mice (Cre-negative, i.e., wild-type DAT littermate mice lacking Cre injected with AAV5-hSyn-FLEX-ChrimsonR-tdTomato; n = 5; Figure 2D). In 6 out of 110 astrocytes, a decrease in the Ca^{2+} signal was observed. Consistent with results found *in vivo,* astrocyte response to opto-stimulation was frequency dependent (Figure S1C).

The astrocyte Ca^{2+} responses to dopamine were abolished by the broad dopamine receptor antagonist flupenthixol (30 μM; n = 125 astrocytes from n = 11 slices for applied dopamine; n = 143 astrocytes from n = 12 slices for opto-stimulation; Figures 2B and 2D), and by the D! receptor antagonist SCH 23390 (5 μM; n = 62 astrocytes from n = 4 slices for applied dopamine; n = 121 astrocytes from n = 6 slices for opto-stimulation; Figures 2B and 2D), but unaffected by the D_2 receptor antagonist sulpiride (10 μM; n = 189 astrocytes from n = 14 slices for applied dopamine; n = 222 astrocytes from n = 13 slices for opto-stimulation; Figures 2B and 2D). Taken together and consistent with ultrastructural evidence, these results indicate that NAc astrocytes express D_1 receptors and respond with Ca^{2+} elevations to synaptically released dopamine through activation of D1 receptors.

Dopamine-Evoked Excitatory Synaptic Regulation Is Mediated by Astrocytes

We next investigated the consequences of the dopamine-induced astrocyte Ca^{2+} elevations on excitatory synaptic transmission in the NAc. We recorded excitatory postsynaptic currents (EPSCs) from medium spiny neurons (MSNs) before, during, and after local application of dopamine while monitoring astrocyte Ca^{2+} levels (Figure 3A). Local application of dopamine, which increased astrocytic Ca^{2+}, transiently depressed EPSC amplitude (from 97.6% ± 2.3% to 74.6% ± 6.2%, n = 9; Figures 3A and 3C and Figures S3A–S3D) (Harvey and Lacey, 1996; Nicola et al., 1996). Likewise, synaptically released dopamine increased astrocytic Ca^{2+} and depressed EPSCs in mice that expressed ChrimsonR (from 98.3% ± 2.6% to 75.6% ± 2%, n = 13; Figures 3B and 3E and Figures S3E–S3H) but did not do so in Cre-negative mice (n = 6; Figure S3H). The dopamine-induced EPSC depression was associated with an enhancement of the paired pulse ratio (PPR) (from 1.1 ± 0.05 to 1.4 ± 0.07, n = 15, for applied dopamine; from 1.04 ± 0.08 to 1.32 ± 0.14, n = 11, for opto-stimulation; Figures S3C and S3G), suggesting a presynaptic

mechanism. For both applied and synaptic dopamine there was a correlation between astrocyte Ca^{2+} elevation changes and percentage of EPSC depression ($r^2 = 0.361$, n = 19 and $r^2 = 0.6214$, n = 11 for applied dopamine and opto-stimulation, respectively; Figures 3D and 3F). Consistent with the effects on astrocyte Ca^{2+}, the synaptic effects were abolished by flupenthixol (n = 6 and n = 4 for applied dopamine and opto-stimulation, respectively; Figures S3D and S3H) and by SCH 23390 (n = 9 and n = 6 for applied dopamine and opto-stimulation, respectively; Figures S3D and S3H), but unaffected by sulpiride (n = 8 and n = 6 for applied dopamine and opto-stimulation, respectively; Figures S3D and S3H). These results indicate that dopamine acts via D_1 -like receptors to presynaptically depress excitatory synaptic transmission (Harvey and Lacey, 1996; Nicola et al., 1996) and that this synaptic regulation is associated with astrocyte Ca^{2+} elevations.

Next, we tested whether the astrocyte activity was necessary for the dopaminergic modulation of excitatory synaptic transmission. We used $IP_3R2^{-/-}$ mice (Li et al., 2005), in which G protein-mediated Ca^{2+} elevations are largely impaired in astrocytes (Gómez-Gonzalo et al.,2015, 2017; Martín et al., 2015; Petravicz et al., 2008). In slices from these mice, astrocyte Ca^{2+} levels and synaptic transmission were both unaffected by dopamine (Ca^{2+}: n = 135 astrocytes from n = 15 slices; EPSC: n = 8; Figure 4B), suggesting that the dopamine-evoked synaptic regulation requires astrocyte activation manifested by the Ca^{2+} signaling. To further test this hypothesis, we selectively ablated G protein signaling in astrocytes by injecting astrocytes through a whole-cell recording pipette with GDPβS (10 mM) (Navarrete and Araque, 2010; Navarrete et al., 2012), a GDP analog that competitively inhibits GTP binding to G proteins and prevents the activation of G protein signaling cascades. In MSNs located within the region of the GDPβS-loaded astrocyte network (Figure 4A), dopamine did not affect astrocyte Ca^{2+} levels (n = 45 astrocytes from n = 4 slices; Figure 4B) or EPSCs (n = 6; Figure 4B). Taken together, these results indicate that activation of G protein signaling in astrocytes is necessary for dopaminergic depression of EPSCs in the NAc.

D_1 Receptors Specifically Expressed in Astrocytes Mediate Dopamine-Evoked Depression of Synaptic Transmission

To specifically examine the contribution of astrocyte D_1 receptors in the NAc, we selectively deleted astroglial D_1 receptors in the NAc by injecting mice containing the D_1 receptor gene floxed (DRD1 flox/flox mice) with AAV8-GFAP-mCherry-Cre into the NAc (GFAP-$D_1^{-/-}$ mice; Figure 4C and Figures S4A and S4B). As controls, virus-injected wild-type littermate mice (i.e., non-floxed DRD1 mice; GFAP-D_1^{WT}) were used. To test the cell specificity of our approach, we examined neuronal sensitivity to D_1 signaling. Cd^{2+}-sensitive neuronal voltage-gated Ca^{2+} currents were depressed by the D_1 agonist SKF 38393 (Surmeier et al., 1995) in both GFAP-D_1^{WT} mice and GFAP-$D_1^{-/-}$ mice (Figures S4C–S4F), indicating that neuronal sensitivity to D_1 signaling remained intact in GFAP-$D_1^{-/-}$ mice.

We next investigated astrocyte responsiveness to dopamine and dopamine-evoked synaptic regulation in GFAP-$D_1^{-/-}$ mice. Dopamine elevated Ca^{2+} in astrocytes from GFAP-D_1^{WT} mice (n = 136 astrocytes, n = 5 slices; Figure 4D) but not in those from GFAP-$D_1^{-/-}$ mice (n = 88 astrocytes, n = 9 slices; Figure 4D). In contrast, astrocytes from both GFAP-D_1^{WT} (n =

133 astrocytes, n = 10 slices; Figure 4D) and GFAP-$D_1^{-/-}$ mice (n = 222 astrocytes from n = 6; Figure 4D) responded to ATP, indicating that the astrocyte Ca^{2+} machinery was preserved. We observed an elevated basal Ca^{2+} event probability in GFAP-$D_1^{-/-}$ mice when compared to GFAP-D_1^{WT} mice (p = 0.006; Table S3), suggesting that tonic D_1 receptor activation regulates basal Ca^{2+} signaling in astrocytes. In addition, the dopamine-evoked synaptic regulation was also absent in GFAP-$D_1^{-/-}$ mice (n = 8; Figure 4E) while remaining present in GFAP-D_1^{WT} mice (n = 8; Figure 4E). These results indicate that D_1 receptors specifically expressed in astrocytes mediate the dopamine-evoked depression of EPSCs in the NAc.

Astrocytes Mediate Synaptic Depression via ATP/ Adenosine Signaling

Adenosine has been proposed to mediate the dopamine-induced synaptic depression in the NAc (Harvey and Lacey, 1997; Kombian et al., 2003; Wang et al., 2012), but the source of adenosine remains unknown. Astrocytes can release different gliotransmitters (Araque et al., 2014), including ATP and its metabolic product adenosine, that regulate synaptic transmission in several brain areas (Martín et al., 2007; Panatier et al., 2011; Pascual et al., 2005; Serrano et al., 2006; Zhang et al., 2003). Therefore, we hypothesized that ATP/ adenosine is the gliotransmitter that mediates the dopamine-induced synaptic regulation. Dopamine-evoked synaptic depression was prevented by the adenosine A_1 receptor antagonist CPT (2 μM; n = 7 and n = 7 for applied dopamine and opto-stimulation, respectively; Figures 5A and 5B), without affecting the astrocyte Ca^{2+} (n = 85 astrocytes from n = 6 slices and n = 60 astrocytes from n = 5 slices for applied dopamine and opto-stimulation, respectively; Figures 5A and 5B). Moreover, exogenous adenosine application (250 μM, 5 s, 0.5 bar) evoked a similar neurotransmission depression to that of dopamine (n = 6 and n = 6, respectively; Figures 5D and 5E), confirming that A_1 receptors mediate depression of EPSCs. Notably in a GDPβS-loaded astrocyte network and in $IP_3R2^{-/-}$ mice, although dopamine was unable to depress excitatory transmission, adenosine depressed the neurotransmission (Figures 5C–5E), indicating that adenosine acts downstream of the astrocyte Ca^{2+} signal. Taken together, these results indicate that dopamine-evoked synaptic depression is mediated by activation of astrocytes, and they suggest sequential mechanisms that involve astrocytic D_1R activation, astrocyte Ca^{2+} elevations, ATP/adenosine release, and activation of presynaptic A_1 receptors (Figure 5F).

Astrocyte Ca^{2+} Elevations Are Sufficient to Depress Excitatory Transmission in the NAc

To further test the involvement of astrocytes in synaptic depression regulation, we investigated if activation of G protein-mediated signaling in astrocytes was sufficient to depress excitatory transmission in the NAc by directly and selectively activating astrocytes using designer receptors exclusively activated by designer drugs (DREADDs). We targeted astrocytes in the NAc with AAV8-GFAP-Gq-DREADD-mCherry (Figure 6A and Figures S5A–S5C). Activation of Gq-DREADD-expressing astrocytes with clozapine-N-oxide (CNO) induced both astrocyte Ca^{2+} elevations (n = 43 astrocytes from n = 8 slices; Figures 6B) and EPSC depression (n = 10; Figures 6C), resulting in an increase in PPR (n = 10; Figure S5D), indicating a presynaptic mechanism. Furthermore, the DREADD-mediated synaptic regulation was prevented by CPT (n = 7; Figure 6C), while the astrocyte Ca^{2+} elevations remained unaffected (n = 32 astrocytes from n = 5 slices; Figure 6B). No changes in astrocytic Ca^{2+} (n = 46 astrocytes from n = 6 slices) or synaptic transmission (n = 6) were

observed in response to CNO in slices from control AAV8-GFAP-mCherry-injected animals (Figures 6B and 6C). Taken together, these results indicate that astrocyte activation depresses excitatory transmission in the NAc via A_1 receptor signaling.

The Psychostimulant Amphetamine Modulates Excitatory Synaptic Transmission through Activation of Astrocytes

The results above indicate that astrocytes are key elements in dopaminergic signaling in the NAc. We then investigated the effects of amphetamine on astrocyte Ca^{2+} signaling and synaptic transmission. Amphetamine (10 μM) increased the Ca^{2+} oscillation frequency in astrocytes (n = 32 astrocytes from n = 6 slices; Figures 7A–7D) and depressed EPSCs (n = 5; Figures 7E–7G). Both effects were blocked by flupenthixol (for Ca^{2+}: n = 34 astrocytes from n = 5 slices, Figure 7D; for EPSCs: n = 5, Figure 7G), indicating the involvement of dopamine receptors. We then tested whether astrocyte activation was necessary for amphetamine actions on EPSCs. We utilized three complementary approaches and found that in slices with GDPβS-loaded astrocytes, and in slices from $IP_3R2^{-/-}$ mice and GFAP-$D_1^{-/-}$ mice, amphetamine-induced astrocyte Ca^{2+} elevations were absent (n = 66 astrocytes, n = 5 slices; n = 96 astrocytes, n = 9 slices; n = 119 astrocytes, n = 11 slices, respectively; Figure 7D) and amphetamine-evoked depression of EPSCs was no longer present (n = 6, n = 6, and n = 5, respectively; Figure 7G). Moreover, amphetamine-induced synaptic depression was abolished by the adenosine A1 receptor antagonist CPT (n = 7; Figure 7G), without affecting Ca^{2+} elevations in astrocytes (n = 109 astrocytes from n = 9, Figure 7D). Taken together, these results indicate that amphetamine acts via the activation of astrocyte D1 receptors and G protein signaling and the subsequent release of ATP/adenosine to depress excitatory synaptic transmission.

Next, we investigated the role of astrocytes on the acute behavioral psychomotor effects of amphetamine. We found that the locomotion enhancement evoked by amphetamine was significantly reduced in $IP_3R2^{-/-}$ mice and GFAP-$D_1^{-/-}$ mice when compared to wild-type controls (Figures 7H and 7I). These results indicate that mice with astrocytes with impaired responses to dopamine also have decreased sensitivity to amphetamine, suggesting that astrocytes contribute to the acute psychomotor behavioral effects of amphetamine.

DISCUSSION

Present results show that astrocytes in the NAc core, a key brain region involved in reward and addiction, respond to synaptically released dopamine *in vivo* and in slices with Ca^{2+} increases mediated by activation of D_1 receptors, which are expressed by astrocytes as evidenced by electronmicroscopy. Furthermore, dopamine, amphetamine, and DREADD activation of astrocytes stimulate the release of ATP/adenosine, which activates neuronal presynaptic A1 receptors and depresses excitatory synaptic transmission. These results indicate that NAc astrocytes are key elements of the dopaminergic system in a brain reward circuit.

In addition to passive support roles, astrocytes have been shown to play crucial roles in mediating synaptic transmission and plasticity in various brain regions such as hippocampus, cortex, amygdala, and dorsal striatum (Covelo and Araque, 2018; Martin-Fernandez et al.,

2017; Martín et al., 2007; Panatier et al., 2011; Pascual et al., 2005). Present findings reveal a key role of astrocytes in the NAc. The astrocyte responsiveness to dopamine through activation of D_1 receptors agrees with previous reports showing that astrocytes respond to dopamine with Ca^{2+} increases in the hippocampus and globus pallidus (Cui et al., 2016; Jennings et al., 2017), and it contrasts with a report that failed to detect Ca^{2+} changes in response to the D_1 receptor agonist SKF 38393 in the NAc (D'Ascenzo et al., 2007).

Astrocytes in the basal ganglia have been suggested to be able to express a variety of dopamine receptors, including D_5 receptors (Brito et al., 2004; Miyazaki et al., 2004). Our results obtained with a genetic approach indicate that the dopamine-evoked astrocyte Ca^{2+} responses are selectively mediated by D_1 receptors. Nevertheless, a potential partial involvement of D_5 receptors, undetected in our experimental conditions, cannot be totally excluded. Likewise, D_2-like receptors in astrocytes have been shown to regulate basal intracellular Ca^{2+} levels in astrocytes in hippocampus and globus pallidus (Cui et al., 2016; Jennings et al., 2017). However, our results indicate that D_2-like receptors do not contribute to the dopamine- or amphetamine-evoked astrocyte Ca^{2+} responses and synaptic regulation in the NAc. Perhaps astrocytes in different brain regions may express different dopamine receptors, or different dopamine receptors serve distinct brain-area-specific signaling.

Present results indicate that D_1-evoked Ca^{2+} increases in astrocytes were mediated by IP_3 signaling, which contrasts with the classical view that D_1-like receptors are coupled to G_s proteins and cAMP production (Beaulieu and Gainetdinov, 2011), but which is consistent with studies showing that D_1-like receptors can also lead to phospholipase C (PLC) activation and intracellular Ca^{2+} increases in an IP_3-dependent manner in cultured neurons (Jin et al., 2003; Lezcano and Bergson, 2002; Tang and Bezprozvanny, 2004) and astrocytes (Zhang et al., 2009), as well as in brain slices (Medvedev et al., 2013). Present results also show that this IP_3-dependent signaling cascade is involved in ATP/adenosine release from astrocytes and mediates both the dopamine synaptic regulation, a phenomenon independent of cAMP levels (Harvey and Lacey, 1997; Nicola et al., 1996), and the amphetamine effects on synaptic transmission and locomotion. Moreover, these results are also consistent with previous reports showing that D_1 receptor activation stimulates PLC and IP_3 production in the striatum in response to amphetamine, cocaine, or apomorphine (Medvedev et al., 2013).

Interestingly, our data show differences in the effectiveness of exogenous application versus synaptic release of dopamine in inducing astrocytic responses (63% and 35% of responding astrocytes, respectively). These differences could be accounted for by the different experimental approaches; indeed, exogenous dopamine application may be more effective in targeting more astrocytes than opto-stimulation of dopaminergic afferents. An alternative explanation for this observation could be that different subpopulations of astrocytes with different abilities to respond to dopamine may exist in the NAc. Further studies, out of the scope of the present work, are required to investigate this exciting question.

Dopamine is known to depress excitatory transmission in the NAc (Bamford et al., 2008; Kalivas and Volkow, 2005); however, the exact mechanism of dopamine-evoked depression was unclear. While some studies have proposed a direct activation of D_1 receptors located in excitatory presynaptic terminals (Harvey and Lacey, 1996; Nicola et al., 1996; Nicola and

Malenka, 1997), other studies have suggested the intermediate signaling molecule ATP/adenosine to mediate dopamine effects in the NAc (Harvey and Lacey, 1997; Kombian et al., 2003; Wang et al., 2012), although the exact source of ATP/adenosine remained unknown. The present results show that dopamine-evoked depression of excitatory synaptic transmission in the NAc is mainly mediated by astrocytic D1 receptors. This is based on the following observations: (1) astrocytes express D_1 receptors; (2) astrocytes respond *in vivo* and in slices to synaptically released dopamine with Ca^{2+} elevations mediated by activation of D1 receptors; (3) dopamine-evoked synaptic depression was absent when astrocyte activation was blocked by GDPβS loading and in $IP_3R2^{-/-}$ mice; and (4) dopamine-evoked synaptic depression was absent in the GFAP-$D_1^{-/-}$ mice that lacked D_1 receptors specifically in astrocytes. In addition, the present results show that selective activation of DREADD-expressing astrocytes depresses synaptic transmission through an A1 receptor-mediated mechanism. Taken together these results indicate that astrocytes release ATP/adenosine downstream of the Ca^{2+} signal. Based on these findings, and reconciling previous apparent contradictory reports, we propose the following mechanistic interpretation of the results: synaptically released dopamine activates D_1 receptors in astrocytes, increasing their intracellular Ca^{2+} and stimulating the release of ATP/adenosine, which acts on presynaptic A_1 receptors to depress excitatory synaptic transmission.

Dopamine regulates excitatory and inhibitory synaptic transmission, plasticity, and neuronal excitability through an extensive number of cellular mechanisms that may not be mutually exclusive (Nicola and Malenka, 1997; Nicola et al., 2000; Tritsch and Sabatini, 2012). The present study reveals a novel mechanism on synaptic regulation by dopamine and amphetamine in which astrocytes and gliotransmission play a critical role. This novel mechanism does not necessarily exclude the existence of other mechanisms underlying synaptic effects of dopamine and amphetamine, such as the regulation of presynaptic conductance (Nicola and Malenka, 1997), modulation of postsynaptic firing (Nicola et al., 2000), or NMDA-dependent long-term synaptic depression (Lüscher and Malenka, 2011). The additional mechanism provided by astrocytes adds further complexity to the diverse synaptic regulatory phenomena underlying reward and addiction

Astrocytes in the NAc have been proposed to regulate neuronal excitability and addiction through the astrocytic release of glutamate in response to mGluR5 stimulation or acute activation with DREADDs (D'Ascenzo et al., 2007; Scofield et al., 2015). While in brain areas such as cortex, hippocampus, or dorsal striatum, astrocytic glutamate has been shown to regulate neurotransmission (see Araque et al., 2014), our results indicate that the regulation of synaptic transmission in the NAc evoked by dopamine and acute activation with DREADDs is mediated by astrocytic ATP/adenosine signaling, which has also been shown to modulate neurotransmission in other brain regions such as retina, cortex, hippocampal CA1, dentate gyrus, and amygdala (Newman, 2004; Martín et al., 2007; Halassa et al., 2009; Di Castro et al., 2011; Panatier et al., 2011; Martin-Fernandez et al., 2017). Although our proposed mechanism for dopamine-evoked synaptic depression involves ATP/adenosine released from astrocytes, it does not necessarily exclude the existence of other gliotransmitters, such as glutamate, which has been shown to be released by NAc astrocytes (Scofield et al., 2015). We have recently reported that single hippocampal astrocytes can release distinct gliotransmitters in response to different neuronal stimuli

(Covelo and Araque, 2018). Hence, it is possible that NAc astrocytes may release both gliotransmitters depending on the input signal received and with different regulatory consequences. Further studies are required to test the possible interaction between glutamate and adenosine release from astrocytes and its physiological consequences in the NAc.

Astrocytes have been proposed to be involved in drug-seeking behavior (Scofield et al., 2015), but the synaptic mechanism of action has not been completely elucidated. Present results show that astrocytes respond to synaptically released dopamine and consequently regulate excitatory neurotransmission through the release of ATP/adenosine and activation of neuronal A_1 adenosine receptors. In addition, they also show that astrocytes are in part responsible for the synaptic effects of the psychostimulant amphetamine. Additionally, the present study shows the first evidence of astrocyte responsiveness to dopamine and amphetamine in freely behaving mice. Our results show that astrocytes are key elements in dopaminergic signaling in the NAc, are modulated by amphetamine, and mediate its actions, indicating that they play critical roles in synaptic regulation in the reward system. Elucidating the cellular mechanisms involved in dopamine neuromodulation is essential for developing efficacious therapies for diseases involving disrupted dopaminergic transmission such as Parkinson's disease and drug addiction. Hence, astrocytes may be potential novel cellular targets for treatment of neuropsychiatric disorders associated with disrupted dopaminergic signaling, such as motivation disorders and drug addiction.

STAR★METHODS

LEAD CONTACT AND MATERIALS AVAILABILITY

This study did not generate new unique reagents. Further information and requests may be directed to and will be fulfilled by the Lead Contact, Dr. Alfonso Araque (araque@umn.edu).

EXPERIMENTAL MODEL AND SUBJECT DETAILS

Ethics Statement—All animal care and sacrifice procedures were approved by the University of Minnesota Institutional Animal Care and Use Committee (IACUC) with compliance to the National Institutes of Health guidelines for the care and use of laboratory animals.

Animals—Mice were housed under 12/12-h light/dark cycle and up to five animals per cage. The following animals (males and females) were used for the present study C57BL/6J, $IP_3R2^{-/-}$ (generously donated by Dr. J. Chen), DRD1 flox/flox (Drd1tm2.1Stl; JAX #025700), DAT-IRES-Cre, GLAST-GCaMP3 (generously donated by Dr. D. Bergles and Dr A. Agarwal). Young (p15-p21) and adult (≥4 weeks) mice were used. GLAST-GCaMP3 mice were generated by crossing R26-lsl-GCaMP3 mice (JAX #014538) (Paukert et al., 2014) with the GLAST-CreERT2 mice (MGI:3830051) (Mori et al., 2006). As CreERT2 protein is inactive in the absence of tamoxifen treatment, expression of GCaMP3 was obtained in adult mice (8 weeks) by 8 daily injections of tamoxifen (1 mg, i.p.), dissolved in 90% sunflower oil, 10% ethanol to a final concentration of 10 mg/mL. The animals were used ≥ 2 weeks after tamoxifen treatment.

METHOD DETAILS

Slice Preparation—Animals were rapidly decapitated and the brain was placed in ice-cold artificial cerebral spinal fluid (ACSF). ACSF contained (in mM): NaCl 124, KCl 2.69, KH_2PO_4 1.25, $MgSO_4$ 2, $NaHCO_3$ 26, $CaCl_2$ 2, and glucose 10, and was oxygenated with 95% O_2 /5% CO_2 (pH = 7.3–7.4). 350 μm thick coronal slices containing the Nucleus Accumbens (NAc) core were made with a vibratome (Leica VT 1200S) and incubated in oxygenated ACSF at room temperature for > 30 min. Slices were placed in an immersion recording chamber and superfused (2 mL/min) with oxygenated ACSF and visualized with an Olympus BX50WI microscope (Olympus Optical, Japan) or an Olympus BX61Wl confocal microscope (Olympus Optical, Japan).

Electrophysiology—The whole-cell patch clamp technique was used to make electrophysiological recordings of NAc core neurons. When filled with an internal solution containing (in mM): $KMeSO_4$ 135, KCl 10, HEPES 10, NaCl 5, ATP-Mg^{+2} 2.5, and GTP-Na^{+} 0.3 (pH = 7.3), patch electrodes exhibited a resistance of 3–10 MΩ. The membrane potential of neurons was held at −70 mV. Series and input resistances were monitored throughout the experiment using a −5 mV pulse. For some experiments, astrocytes were patched with 4–9 MΩ electrodes filled with an internal solution containing (in mM): $KMeSO_4$ 100, KCl 50, HEPES-K 10, and ATP-Na^{+2} 4 (pH = 7.3). Astrocytes membrane potential was held at −80 mV. GDPβS (10 mM) and 0.5% biocytin were included in the astrocyte patch pipette. GDPβS was included to prevent G protein-mediated intracellular signaling in astrocytes. Astrocyte whole-cell recordings lasted at least 15–25 min to allow the dialysis of GDPβS throughout the gap-junction connected astrocyte network. Then, a relatively distant neuron (> 60 μm away from the recorded astrocyte) within the same field of view was patch-clamp recorded to monitor EPSCs (Navarrete and Araque, 2010). Signals were recorded with PC-ONE amplifiers (Dagan Instruments, MN, US) and fed to a Pentium-based PC through a DigiData 1440A interface board. Signals were filtered at 1 KHz and acquired at 10 KHz sampling rate. The pCLAMP 10.4 (Axon instruments) software was used for stimulus generation, data display, acquisition and storage.

Synaptic stimulation and drug application—Synaptic currents were evoked using bipolar theta capillaries filled with ACSF placed in the brain region of study (NAc core). Paired pulses (2 ms duration with 50 ms interval) were continuously delivered at 0.33 Hz using a stimulator S-910 through an isolation unit. Excitatory post-synaptic currents (EPSCs) were isolated using picrotoxin (50 μM) and CGP5462 (1 μM) to block $GABA_AR$ and $GABA_bR$, respectively. The measures analyzed were mean amplitude of EPSC response and paired pulse ratio (PPR = 2^{nd} EPSC/1^{st} EPSC). For exogenous dopamine (500 μM), adenosine (250 μM) and CNO (1 mM) application, a borosilicate glass pipette containing the drug was placed over the NAc core and it was applied with a pressure pulse (0.5 bar, 5 s). For SKF 38393 application a borosilicate glass pipette containing SKF 38393 (500 μM) was placed over the NAc core and it was applied with a pressure pulse (0.5 bar, 60 s). For optical stimulation of dopamine axons, an optic fiber connected to an LED (620 nm) was placed over the NAc core and a light train (5ms pulses for 5 s) of 0.1, 1, 10, 20, 30 or 50 Hz was applied. EPSC amplitudes were grouped in 15 s time bins, baseline mean EPSC amplitude was obtained by averaging mean values obtained within 2 min of baseline recordings and

mean EPSC amplitudes were normalized to baseline. Stimulus (dopamine, CNO or optostimulation) effects were statistically tested comparing the normalized EPSCs recorded 15 s before and after the stimulus to assess changes in EPSC amplitude and PPR. For amphetamine experiments, EPSC amplitudes were grouped in 1 min time bins and EPSC obtained 1 min before and 20 min after amphetamine were compared to assess changes in EPSC amplitude. The effects of the pharmacological compounds on dopamine, CNO or optostimulation application were tested after having performed the stimulation in control conditions (dopamine, CNO or optostimulation without the pharmacological compound).

***In vitro* Ca^{2+} imaging—**Cytoplasmic Ca^{2+} levels in astrocytes in the NAc core were monitored using epifluorescence and confocal microscopy. Epifluorescence imaging utilized a CCD camera (Hammamatsu, Japan). Cells were illuminated during 100–200 ms with an LED at 490 nm (Prior Scientifics, MA, US) and images were acquired every 1–2 s. The LED and the CCD camera were controlled and synchronized by the MetaMorph software (Molecular devices). Confocal imaging utilized an Olympus BX61Wl confocal microscope (Olympus Optical, Japan) controlled by the Fluoview software or a Leica SP5 multi-photon microscope (Leica Microsystems, USA) controlled by the Leica LAS software. For control and pharmacology experiments Ca^{2+} was monitored using the genetically encoded Ca^{2+} indicator dye GCaMP3 under the glutamate aspartate transporter (GLAST) promoter (Figures S2A and S2B). For transgenic mice, that did not constitutively express GCaMP3, we used GCaMP6 under the GfaABC1D promoter to specifically target astrocytes (Figure S2C) or Fluo4. For experiments using fluo-4, slices were incubated with fluo-4-AM (2 μM and 0.01% of pluronic) for 60 min at room temperature. Where noted, Ca^{2+} experiments were performed in the presence of TTX (1 μM) and a cocktail of neurotransmitter receptor antagonists containing: CNQX (20 μM), AP5 (50 μM), MPEP (50 μM), LY367385 (100 μM), picrotoxin (50 μM), CGP5462 (1 μM), atropine (50 μM), CPT (10 μM), and suramin (100 μM). TTX (1 μM) was always present in Ca^{2+} imaging experiments testing exogenous dopamine or amphetamine application, but not in experiments using optogenetic stimulation or assessing synaptic transmission.

ImageJ software (NIH) was used to quantify fluorescence level measurements in astrocytes. Ca^{2+} variations recorded at the soma and processes of the cells were estimated as changes of the fluorescence signal over baseline ($\Delta F/F_0$), and cells were considered to show a Ca^{2+} event when the $\Delta F/F_0$ increase was at least two times the standard deviation of the baseline and the astrocyte was considered to respond to the stimulus if the Ca^{2+} event occurred within 10 s after the stimulation. The astrocyte Ca^{2+} signal was quantified from the Ca^{2+} event probability, which was calculated from the number of Ca^{2+} elevations grouped in 10 s bins recorded from 2–50 astrocytes per field of view. The time of occurrence was considered at the onset of the Ca^{2+} event. For each astrocyte analyzed, values of 0 and 1 were assigned for bins showing either no response or a Ca^{2+} event, respectively, and the Ca^{2+} event probability was obtained by dividing the number of astrocytes showing an event at each time bin by the total number of monitored astrocytes. To examine the difference in Ca^{2+} event probability in distinct conditions, the basal Ca^{2+} event probability (10 s before a stimulus) was averaged and compared to the average Ca^{2+} event probability (10 s after a stimulus). The Ca^{2+} oscillation frequency was used for amphetamine experiments due to the mechanism of

action of amphetamine and the evaluation of Ca^{2+} oscillations over a minute-timescale. In slice experiments using amphetamine (10 μM), the astrocyte Ca^{2+} signal was quantified from the Ca^{2+} oscillation frequency, which was obtained from the number of Ca^{2+} events occurring in 2–50 astrocytes per the field of view during 1 min periods. To establish magnitude correlations in Figures 3D and 3F, we examined the maximum values of the Ca^{2+} event probability and EPSC depression occurring within 15 s after the stimulation.

Stereotaxic Surgery—Adult mice were anesthetized with a ketamine (100 mg/kg)/xylazine (10mg/kg) cocktail. Viral vectors (0.5 μl-1 μl) were injected bilaterally using a Hamilton syringe attached to a 29-gauge needle at a rate of 0.8–1.25 μl/min. The viral constructs AAV8-GFAP-hM3D(Gq)-mCherry (UNC vector core), AAV8-GFAP-mCherry (UMN vector core), AAV5-GfaABC1D-PI-LckGCaMP6.SV40 (Penn Vector Core), or AAV5-GfaABC1D-cytoGCaMP6f-SV40 (Penn Vector Core) were targeted to NAc core astrocytes (anterior-poste- rior[AP]: +1.50 mm; medial-lateral [ML]: +/− 0.75 mm; dorsal-ventral [DV]: −4.50 mm) of C57BL/6J. The AAV8-GFAP-mCherry- Cre viral vector (UNC vector core) was targeted to NAc core astrocytes of DRD1 flox/flox mice (homozygous and wild-type littermate mice). The AAV5-hSyn-FLEX-ChrimsonR-tdT (UNC vector core) was targeted to dopaminergic neurons in the VTA of DAT-IRES-Cre mice and wild-type littermate mice (anterior-posterior [AP]: −3 mm; medial-lateral [ML]: +/− 0.5 mm; dorsal-ventral [DV]: −4.3 mm). For some experiments, AAV5-GfaABC1D-PI-LckGCaMP6.SV40 (Penn Vector Core) or AAV5-GfaABC1D-cytoGCaMP6f-SV40 (Penn Vector Core) was also injected in the NAc core of DAT-IRES-Cre mice to monitor astrocyte Ca^{2+} signals. Mice were used ≥ 2 weeks after stereotaxic surgeries. The viral vectors and mouse genotypes used for generating transgenic mice and their controls are reported in Table S4.

Fiber Photometry—We utilized fiber photometry to assess astrocyte Ca^{2+} activity and responsiveness to dopamine and amphetamine in freely behaving mice. In DAT-IRES-Cre mice, AAV5-hSyn-FLEX-ChrimsonR-tdT (0.5 μl; UNC vector core) was targeted to dopaminergic neurons in the VTA (anterior-posterior [AP]: −3 mm; medial-lateral [ML]: +/− 0.5 mm; dorsal-ventral [DV]: −4.3 mm) and AAV5-GfaABC1D-cytoGCaMP6f-SV40 (1 μl; Penn Vector Core) or AAV5-GfaABC1D-PI-Lck-GFP-SV40 (1 μl; addgene) was targeted to NAc core astrocytes (anterior-posterior[AP]: +1.50 mm; medial-lateral [ML]: +/− 0.75 mm; dorsal-ventral [DV]: −4.50 mm) and the optic fiber (400 μm, Doric Lenses: MFC_400/430–0.48_6mm_MF2.5_FLT) was placed 0.02 mm dorsal to NAc core viral infusion. The implant was attached to the skull with a dual-cure resin-ionomer (DenMat). Experiments were performed > 3 weeks after surgery.

For data acquisition, the RZ5P processor (Tucker Davis Technologies) was utilized. A fluorescence mini-cube (Doric Lenses) was coupled to a 470 nm LED (Thorlabs M470F3; modulated at 211 Hz), a 405 nm LED (Thorlabs M405F1; modulated at 531 Hz) and a 595 nm LED (Thorlabs M595F2; for optogenetic stimulation of dopaminergic terminals expressing ChrimsonR). The fluorescence mini-cube was coupled to a patch cable and the opposite end was connected to the implanted optic fiber on the mice. GCaMP6f fluorescence from astrocytes was transmitted back through the cable to the mini-cube and focused onto the photoreceiver (Newport Model 2151, FC adaptor). The sampling rate for the signals was

6.1 kHz. For each stimulation parameter (5 ms pulses for 5 s at 5,10, 20, 30 or 50 Hz) mice were stimulated 3–5 times with a 2 min inter-stimulation interval. For analysis, individual stimulations from control and pharmacological conditions (flupenthixol or amphetamine) were averaged and compared.

For data analysis, active (470 nm) and reference (405 nm) photometry signals were corrected for bleaching by fitting to an exponential function. The normalized signal was created via examining change in fluorescence ([470nm signal - fitted 405nm signal]/[fitted 405nm signal]). Custom MATLAB code (Data S1) was utilized to analyze the normalized data.

Brains from all mice used in fiber photometry experiments were analyzed to check adequate fiber location and proper and selective viral expression. Animals that did not meet the criteria for proper fiber location and virus expression were discarded.

Acute amphetamine locomotor-sensitivity—Male and female $IP_3R2^{-/-}$ mice (n = 18; n = 8 males and n = 10 females), $IP_3R2^{-/-}$ control wild-type background mice (Black Swiss; n = 16; n = 5 males and n = 11 females), GFAP-$D_1^{-/-}$ mice (n = 6; n = 3 males and n = 3 females;) and GFAP-D_1^{WT} (n = 6; n = 3 males and n = 3 females) were used for behavioral experiments. Mice were ≥ 5 weeks of age. Mice were handled by experimenter for at least two days before behavioral testing commenced. To habituate animals to i.p. injections and experimental conditions, mice were injected with saline for two consecutive days. On experimental day, mice were injected with amphetamine (2.5 mg/kg, i.p. for $IP_3R2^{-/-}$ mice and 5 mg/kg for GFAP-$D1^{-/-}$ mice experiments). On test days, mice were placed in locomotor chambers for 30 min to habituate to the environment, followed by drug administration (saline or amphetamine) and 60 min of locomotor tracking post-injection. Locomotor activity was tracked automatically using a camera tracking system and ANY-maze software (Stoelting Co.). A two-way repeated-measures ANOVA was used to analyze the data.

Immunohistochemistry—The animals were anesthetized with Avertin (2,2,2 tribromoethanol, 240 mg/kg, i.p.) and intracardially perfused with ice cold phosphate buffered saline (PBS) and subsequently with 4% paraformaldehyde (PFA) in 0.1 M phosphate buffered saline (pH 7.4). The brain was removed and 40 mm coronal sections were made using a Leica VT1000S vibratome. Vibratome sections were incubated for one h in blocking buffer (0.1% Triton X-100,10% Donkey or Goat serum in PBS) at room temperature. The primary antibodies were diluted in the blocking solution and the sections were incubated overnight at 4°C. The following primary antibodies were used: Sheep anti-TH (Pel-Freez, 1:500), Mouse anti-NeuN (Millipore, 1:500), Rabbit anti-NeuN (Millipore; 1:500), Rabbit anti-GFAP (Sigma, 1:500), Mouse anti-NG2 (Millipore; 1:500), Rabbit anti-Iba1 (Dako; 1:500). The slices were washed three times forten minutes each in 0.1M PBS. The secondary antibodies were diluted in the secondary antibody buffer (0.1% Triton X-100,5% Donkey or Goat serum in PBS) and incubated for 2 h at room temperature. The following secondary antibodies were used: 488 donkey anti-sheep (Invitrogen, 1:500), 405 goat anti-mouse (Invitrogen, 1:500) 488 goat anti-rabbit (Invitrogen, 1:1000). The sections were then washed 3 times with 1xPBS for 10 min each and mounted using Vectashield

Mounting media (Vector laboratories). Mounted slices were imaged using a Leica SP5 multi-photon microscope.

The cellular specificity of GCaMP3, GCaMP6, DREADD and Cre viral vectors was tested by immohistochemical analysis of randomly selected areas of the NAc. Out of the 511 cells expressing GCaMP3 from GLAST-GCaMP3 mice, 99% were astrocytes (identified by GFAP), 0.6% were neurons (identified by NeuN), 0% were oligodendrocytes (identified by NG2) and 0.4% were microglia (identified by Iba1) (Figures S2A and S2B). Out of the 192 cells expressing GCaMP6 from the AAV5-GfaABC1D-cytoGCaMP6f- SV40 viral vector, 99% were astrocytes (identified by GFAP), 0% were neurons (identified by NeuN), 0% were oligodendrocytes (identified by NG2) and 1% were microglia (identified by Iba1) (Figure S2C). Out of the 408 cells expressing mCherry from the AAV8-GFAP-hM3D(Gq)-mCherry viral vector, 99.01% were astrocytes (identified by GFAP), 0.25% were neurons (identified by NeuN), 0% were oligodendrocytes (identified by NG2) and 0.74% were microglia (identified by Iba1) (Figures S5A–S5C). Out of the 985 cells expressing mCherry from the AAV8-GFAP-mCherry-Cre viral vector, 87.6% were astrocytes (identified by GFAP), 11.9% were neurons (identified by NeuN), 0% were oligodendrocytes (identified by NG2) and 0.5% were microglia (identified by Iba1) (Figures S4A and S4B).

For biocytin labeling single astrocytes were recorded with patch pipettes and filled with internal solution containing 0.5% biocytin. Slices were fixed in 4% PFA in 0.1 PBS (pH 7.4) at 4°C. Slices were washed three times in 1xPBS (10 min each). To visualize biocytin slices were incubated with Alexa488-Streptavidin (RRID: AB 2315383; 1:500) for 48 h at4°C. Slices were then washed for 3 times with 1xPBS (10 min each) and mounted with Vectashield mounting media (Vector laboratories). All mounted slices were imaged using a Leica SP5 multi-photon microscope. The cellular specificity of biocytin labeling was assessed by immohistochemical analysis of randomly selected areas of the NAc. Out of 127 cells expressing biocytin, 5% were oligodendrocytes (identified by NG2).

Tissue preparation for electron microscopy—Three mice, obtained from the Animal House Facility (School of Medicine, University of Castilla-La Mancha), were used in this study for pre-embedding immunohistochemical analyses. The care and handling of animals prior to and during the experimental procedures were in accordance with Spanish (RD 1201/2005) and European Union (86/609/EC) regulations, and the protocols were approved by the University's Animal Care and Use Committee.

Animals were anaesthetized by intraperitoneal injection of ketamine/xylazine 1:1 (0.1 mL/kg b.w.) and transcardially perfused with ice-cold fixative containing 4% paraformaldehyde, with 0.05% glutaraldehyde and 15% (v/v) saturated picric acid made up in 0.1 M phosphate buffer (PB, pH 7.4). After perfusion, brains were removed and immersed in the same fixative for 2 h or overnight at 4°C. Tissue blocks were washed thoroughly in 0.1 M PB. Coronal 60 μm thick sections were cut on a Vibratome (Leica V1000).

Antibodies and chemicals for electron microscopy—The following primary antibodies were used: guinea pig anti-D1R polyclonal (GP-Af500; C terminus 45 aa. of mouse D1R, NM010076; Frontier Institute co., Japan). The characteristics and specificity of

the antibody targeting D1R has been described elsewhere (Nar- ushima et al., 2006; Uchigashima et al., 2007). The secondary antibodies used were goat anti-guinea pig IgG coupled to 1.4 nm gold (1:100; Nanoprobes Inc., Stony Brook, NY, USA).

Immunohistochemistry for electron microscopy—Immunohistochemical reactions for electron microscopy were carried out using the pre-embedding immunogold method described previously (Lujan et al., 1996). Briefly, free-floating sections were incubated in 10% (v/v) NGS diluted in TBS. Sections were then incubated in anti-D1R antibodies [3–5 μg/mL diluted in TBS containing 1% (v/v) NGS], followed by incubation in goat anti-guinea pig IgG coupled to 1.4 nm gold (Nanoprobes Inc., Stony Brook, NY, USA), respectively. Sections were postfixed in 1% (v/v) glutaraldehyde and washed in double-distilled water, followed by silver enhancement of the gold particles with an HQ Silver kit (Nanoprobes Inc.). Sections were then treated with osmium tetraoxide (1% in 0.1 m phosphate buffer), block-stained with uranyl acetate, dehydrated in graded series of ethanol and flat-embedded on glass slides in Durcupan (Fluka) resin. Regions of interest were cut at 70–90 nm on an ultramicrotome (Reichert Ultracut E, Leica, Austria) and collected on single slot pioloform-coated copper grids. Staining was performed on drops of 1% aqueous uranyl acetate followed by Reynolds's lead citrate. Ultrastructural analyses were performed in a Jeol-1010 electron microscope.

Drugs—4-[3-[2-(Trifluoromethyl)-9*H*-thioxanthen-9-ylidene]propyl]-1-piperazineethanol dihydrochloride (flupenthixol dihydrochloride), [*S*-(*R**,*R**)]-[3-[[1-(3,4-Dichlorophenyl)ethyl]amino]-2-hydroxypropyl](cyclohexylmethyl) phosphinic acid (CGP 54626 hydrochloride), 8,8'-[Carbonyl*bis*[imino-3,1-phenylenecarbonylimino(4-methyl-3,1-phenylene)carbonylimino]]*bis*-1,3,5-naphthalenetrisulfonic acid hexasodium salt (suramin hexasodium salt), *N*-(Piperidin-1-yl)-5-(4-iodophenyl)-1-(2,4-dichlorophenyl)-4-methyl-1*H*-pyrazole-3-carboxamide (AM 251), D-(−)-2-Amino-5-phosphonopentanoic acid (D-AP5), 6-Cyano-7-nitroquinoxaline-2,3-dione disodium (CNQX disodium salt), (*S*)-(+)-α-Amino-4-carboxy-2-methylbenzeneacetic acid (LY367385), and 2-Methyl-6-(phenylethynyl)pyridine hydrochloride (MPEP hydrochloride), Octahydro-12-(hydroxymethyl)-2-imino-5,9:7,10a-dimethano-10a*H*-[1,3]dioxocino[6,5-*d*]pyrimidine-4,7,10,11,12-pentol (Tetrodotoxin: TTX) were purchased from Tocris Bioscience. Picrotoxin from Indofine Chemical Company (Hillsborough, NJ). Fluo-4-AM from Molecular Probes (Eugene, OR). All other drugs were purchased from Sigma.

QUANTIFICATION AND STATISTICAL ANALYSIS

The data generated during this study is detailed in Table S5. Data are expressed as mean ± standard error of the mean (SEM). For electrophysiology comparisons number of neurons was used as the sample size; for *in vitro* Ca^{2+} signal comparisons the number of slices was used as the sample size; for fiber photometry and behavior comparisons the number of mice was used as the sample size. At least 3 mice per experimental group were used. Data normality was tested using a Kolmogorov-Smirnov test. Results were compared using a two-tailed Student's t test or ANOVA ($\alpha = 0.05$). One-way ANOVA with a Fisher LSD method post hoc was used for normal distributed data and Kruskal-Wallis One-Way ANOVA with Dunn's method post hoc was used for non-normal distributed data. A full report of the

statistics used in every case is detailed in Tables S1, S2, and S3. Statistical differences were established with $p < 0.05$ (*), $p < 0.01$ (**) and $p < 0.001$ (***).

DATA AND CODE AVAILABILITY

The published article includes all MATLAB code generated for analysis (Data S1) and the data supporting the conclusions of this study (Table S5). Further information is available under request to the Lead Contact Dr. Alfonso Araque (araque@umn.edu).

Supplementary Material

Refer to Web version on PubMed Central for supplementary material.

ACKNOWLEDGMENTS

We thank C. Nanclares, F.E. Labrada-Moncada, D. Deters, and S. Jamison for technical assistance and members of the Thomas lab and Araque lab for helpful suggestions. We thank E. Larson and the MnDRIVE Optogenetics Core at the University of Minnesota for academic and technical support and the acquisition of the fiber photometry system. We thank T. Nichols-Meade and M. Benneyworth at the Mouse Behavior Core, University of Minnesota and the personnel of the Animal Facility of NeuroCentre Magendie for academic and technical support. Work was done using a Leica SP5 multi-photon microscope at the University of Minnesota – University Imaging Centers. We thank the University of Minnesota Viral Vector and Cloning Core for production of some of the viral vectors used in this study. This work was supported by NIH-NIDA (1F30DA042510.01) to M.C., IdEx University of Bordeaux Investments for the Future program (France) to A.C., NIH-NINDS (R01NS097312) and NIH-NIDA (R01DA048822) to A.A., INSERM and European Research Council (MiCaBra, ERC-2017-AdG-786467) to G.M., Human Frontier Science Program (Research Grant RGP0036/2014) to A.A. and G.M., Salvador de Madariaga Program (Spain) to E.D.M., and ANR JCJC (mitoCB1-fat) to L.B.

REFERENCES

Araque A, Parpura V, Sanzgiri RP, and Haydon PG (1999). Tripartite synapses: glia, the unacknowledged partner. Trends Neurosci. 22, 208–215. [PubMed: 10322493]

Araque A, Carmignoto G, and Haydon PG (2001). Dynamic signaling between astrocytes and neurons. Annu. Rev. Physiol 63, 795–813. [PubMed: 11181976]

Araque A, Carmignoto G, Haydon PG, Oliet SH, Robitaille R, and Volterra A (2014). Gliotransmitters travel in time and space. Neuron 81, 728–739. [PubMed: 24559669]

Bamford NS, Zhang H, Joyce JA, Scarlis CA, Hanan W, Wu NP, André VM, Cohen R, Cepeda C, Levine MS, et al. (2008). Repeated exposure to methamphetamine causes long-lasting presynaptic corticostriatal depression that is renormalized with drug readministration. Neuron 58, 89–103. [PubMed: 18400166]

Beaulieu JM, and Gainetdinov RR (2011). The physiology, signaling, and pharmacology of dopamine receptors. Pharmacol. Rev 63, 182–217. [PubMed: 21303898]

Bezzi P, Gundersen V, Galbete JL, Seifert G, Steinhäuser C, Pilati E, and Volterra A (2004). Astrocytes contain a vesicular compartment that is competent for regulated exocytosis of glutamate. Nat. Neurosci 7, 613–620. [PubMed: 15156145]

Brito V, Beyer C, and Küppers E (2004). BDNF-dependent stimulation of dopamine D5 receptor expression in developing striatal astrocytes involves PI3-kinase signaling. Glia 46, 284–295. [PubMed: 15048851]

Calipari ES, and Ferris MJ (2013). Amphetamine mechanisms and actions at the dopamine terminal revisited. J. Neurosci 33, 8923–8925. [PubMed: 23699503]

Covelo A, and Araque A (2016). Lateral regulation of synaptic transmission by astrocytes. Neuroscience 323, 62–66. [PubMed: 25732135]

Covelo A, and Araque A (2018). Neuronal activity determines distinct gliotransmitter release from a single astrocyte. eLife 7, 10.7554/Life.32237.

Cui Q, Pitt JE, Pamukcu A, Poulin JF, Mabrouk OS, Fiske MP, Fan IB, Augustine EC, Young KA, Kennedy RT, et al. (2016). Blunted mGluR Activation Disinhibits Striatopallidal Transmission in Parkinsonian Mice. Cell Rep. 17, 2431–2444. [PubMed: 27880915]

D'Ascenzo M, Fellin T, Terunuma M, Revilla-Sanchez R, Meaney DF, Auberson YP, Moss SJ, and Haydon PG (2007). mGluR5 stimulates gliotransmission in the nucleus accumbens. Proc. Natl. Acad. Sci. USA 104, 1995–2000. [PubMed: 17259307]

Di Castro MA, Chuquet J, Liaudet N, Bhaukaurally K, Santello M, Bouvier D, Tiret P, and Volterra A (2011). Local Ca2+ detection and modulation of synaptic release by astrocytes. Nat. Neurosci 14, 1276–1284. [PubMed: 21909085]

Gómez-Gonzalo M, Navarrete M, Perea G, Covelo A, Martín-Fernández M, Shigemoto R, Luján R, and Araque A (2015). Endocannabinoids Induce Lateral Long-Term Potentiation of Transmitter Release by Stimulation of Gliotransmission. Cereb. Cortex 25, 3699–3712. [PubMed: 25260706]

Gómez-Gonzalo M, Martin-Fernandez M, Martínez-Murillo R, Mederos S, Hernández-Vivanco A, Jamison S, Fernandez AP, Serrano J, Calero P, Futch HS, et al. (2017). Neuron-astrocyte signaling is preserved in the aging brain. Glia 65, 569–580. [PubMed: 28130845]

Halassa MM, Florian C, Fellin T, Munoz JR, Lee S-Y, Abel T, Haydon PG, and Frank MG (2009). Astrocytic modulation of sleep homeostasis and cognitive consequences of sleep loss. Neuron 61, 213–219. [PubMed: 19186164]

Halassa MM, and Haydon PG (2010). Integrated brain circuits: astrocytic networks modulate neuronal activity and behavior. Annu. Rev. Physiol 72, 335–355. [PubMed: 20148679]

Harvey J, and Lacey MG (1996). Endogenous and exogenous dopamine depress EPSCs in rat nucleus accumbens in vitro via D1 receptors activation. J. Physiol 492, 143–154. [PubMed: 8730590]

Harvey J, and Lacey MG (1997). A postsynaptic interaction between dopamine D1 and NMDA receptors promotes presynaptic inhibition in the rat nucleus accumbens via adenosine release. J. Neurosci 17, 5271–5280. [PubMed: 9204911]

Haydon PG, and Carmignoto G (2006). Astrocyte control of synaptic transmission and neurovascular coupling. Physiol. Rev 86, 1009–1031. [PubMed: 16816144]

Henneberger C, Papouin T, Oliet SH, and Rusakov DA (2010). Long-term potentiation depends on release of D-serine from astrocytes. Nature 463, 232–236. [PubMed: 20075918]

Jennings A, Tyurikova O, Bard L, Zheng K, Semyanov A, Henneberger C, and Rusakov DA (2017). Dopamine elevates and lowers astroglial Ca^{2+} through distinct pathways depending on local synaptic circuitry. Glia 65, 447–459. [PubMed: 27896839]

Jin LQ, Goswami S, Cai G, Zhen X, and Friedman E (2003). SKF83959 selectively regulates phosphatidylinositol-linked D1 dopamine receptors in rat brain. J. Neurochem 85, 378–386. [PubMed: 12675914]

Kalivas PW, and Volkow ND (2005). The neural basis of addiction: a pathology of motivation and choice. Am. J. Psychiatry 162, 1403–1413. [PubMed: 16055761]

Klapoetke NC, Murata Y, Kim SS, Pulver SR, Birdsey-Benson A, Cho YK, Morimoto TK, Chuong AS, Carpenter EJ, Tian Z, et al. (2014). Independent optical excitation of distinct neural populations. Nat. Methods 11, 338–346. [PubMed: 24509633]

Kombian SB, Ananthalakshmi KV, Parvathy SS, and Matowe WC (2003). Substance P depresses excitatory synaptic transmission in the nucleus accumbens through dopaminergic and purinergic mechanisms. J. Neurophysiol 89, 728–737. [PubMed: 12574450]

Lerner TN, Shilyansky C, Davidson TJ, Evans KE, Beier KT, Zalocusky KA, Crow AK, Malenka RC, Luo L, Tomer R, and Deisseroth K (2015). Intact-Brain Analyses Reveal Distinct Information Carried by SNc Dopamine Subcircuits. Cell 162, 635–647. [PubMed: 26232229]

Lezcano N, and Bergson C (2002). D1/D5 dopamine receptors stimulate intracellular calcium release in primary cultures of neocortical and hippocampal neurons. J. Neurophysiol 87, 2167–2175. [PubMed: 11929934]

Li X, Zima AV, Sheikh F, Blatter LA, and Chen J (2005). Endothelin-1-induced arrhythmogenic Ca2+ signaling is abolished in atrial myocytes of inositol-1,4,5-trisphosphate(IP3)-receptor type 2-deficient mice. Circ. Res 96, 1274–1281. [PubMed: 15933266]

Lujan R, Nusser Z, Roberts JD, Shigemoto R, and Somogyi P (1996). Perisynaptic location of metabotropic glutamate receptors mGluR1 and mGluR5 on dendrites and dendritic spines in the rat hippocampus. Eur. J. Neurosci 8, 1488–1500. [PubMed: 8758956]

Lüscher C (2016). The Emergence of a Circuit Model for Addiction. Annu. Rev. Neurosci 39, 257–276. [PubMed: 27145911]

Lüscher C, and Malenka RC (2011). Drug-evoked synaptic plasticity in addiction: from molecular changes to circuit remodeling. Neuron 69, 650–663. [PubMed: 21338877]

Martín ED, Fernández M, Perea G, Pascual O, Haydon PG, Araque A, and Ceña V (2007). Adenosine released by astrocytes contributes to hypoxia-induced modulation of synaptic transmission. Glia 55, 36–45. [PubMed: 17004232]

Martín R, Bajo-Grarñeras R, Moratalla R, Perea G, and Araque A (2015). Circuit-specific signaling in astrocyte-neuron networks in basal ganglia pathways. Science 349, 730–734. [PubMed: 26273054]

Martin-Fernandez M, Jamison S, Robin LM, Zhao Z, Martin ED, Aguilar J, Benneyworth MA, Marsicano G, and Araque A (2017). Synapse-specific astrocyte gating of amygdala-related behavior. Nat. Neurosci 20, 1540–1548. [PubMed: 28945222]

Medvedev IO, Ramsey AJ, Masoud ST, Bermejo MK, Urs N, Sotnikova TD, Beaulieu J-M, Gainetdinov RR, and Salahpour A (2013). D1 dopamine receptor coupling to PLCβ regulates forward locomotion in mice. J. Neurosci 33, 18125–18133. [PubMed: 24227722]

Min R, and Nevian T (2012). Astrocyte signaling controls spike timing-dependent depression at neocortical synapses. Nat. Neurosci 15, 746–753. [PubMed: 22446881]

Min R, Santello M, and Nevian T (2012). The computational power of astrocyte mediated synaptic plasticity. Front. Comput. Neurosci 6, 93. [PubMed: 23125832]

Miyazaki I, Asanuma M, Diaz-Corrales FJ, Miyoshi K, and Ogawa N (2004). Direct evidence for expression of dopamine receptors in astrocytes from basal ganglia. Brain Res. 1029, 120–123. [PubMed: 15533323]

Mori T, Tanaka K, Buffo A, Wurst W, Kühn R, and Götz M (2006). Inducible gene deletion in astroglia and radial glia–a valuable tool for functional and lineage analysis. Glia 54, 21–34. [PubMed: 16652340]

Narushima M, Uchigashima M, Hashimoto K, Watanabe M, and Kano M (2006). Depolarization-induced suppression of inhibition mediated by endo-cannabinoids at synapses from fast-spiking interneurons to medium spiny neurons in the striatum. Eur. J. Neurosci 24, 2246–2252. [PubMed: 17042791]

Navarrete M, and Araque A (2010). Endocannabinoids potentiate synaptic transmission through stimulation of astrocytes. Neuron 68, 113–126. [PubMed: 20920795]

Navarrete M, Perea G, Fernandez de Sevilla D, Gómez-Gonzalo M, Núñez A, Martín ED, and Araque A (2012). Astrocytes mediate in vivo cholinergic-induced synaptic plasticity. PLoS Biol. 10, e1001259. [PubMed: 22347811]

Nicola SM, and Malenka RC (1997). Dopamine depresses excitatory and inhibitory synaptic transmission by distinct mechanisms in the nucleus accumbens. J. Neurosci 17, 5697–5710. [PubMed: 9221769]

Newman EA (2004). Glial modulation of synaptic transmission in the retina. Glia 47, 268–274. [PubMed: 15252816]

Nicola SM, Kombian SB, and Malenka RC (1996). Psychostimulants depress excitatory synaptic transmission in the nucleus accumbens via presynaptic D1-like dopamine receptors. J. Neurosci 16, 1591–1604. [PubMed: 8774428]

Nicola SM, Surmeier J, and Malenka RC (2000). Dopaminergic modulation of neuronal excitability in the striatum and nucleus accumbens. Annu. Rev. Neurosci 23, 185–215. [PubMed: 10845063]

Panatier A, Vallée J, Haber M, Murai KK, Lacaille JC, and Robitaille R (2011). Astrocytes are endogenous regulators of basal transmission at central synapses. Cell 146, 785–798. [PubMed: 21855979]

Parri HR, Gould TM, and Crunelli V (2001). Spontaneous astrocytic Ca2+ oscillations in situ drive NMDAR-mediated neuronal excitation. Nat. Neurosci 4, 803–812. [PubMed: 11477426]

Pascual O, Casper KB, Kubera C, Zhang J, Revilla-Sanchez R, Sul JY, Takano H, Moss SJ, McCarthy K, and Haydon PG (2005). Astrocytic purinergic signaling coordinates synaptic networks. Science 310, 113–116. [PubMed: 16210541]

Paukert M, Agarwal A, Cha J, Doze VA, Kang JU, and Bergles DE (2014). Norepinephrine controls astroglial responsiveness to local circuit activity. Neuron 82, 1263–1270. [PubMed: 24945771]

Perea G, and Araque A (2007). Astrocytes potentiate transmitter release at single hippocampal synapses. Science 317, 1083–1086. [PubMed: 17717185]

Perea G, Navarrete M, and Araque A (2009). Tripartite synapses: astrocytes process and control synaptic information. Trends Neurosci. 32, 421–431. [PubMed: 19615761]

Perea G, Gómez R, Mederos S, Covelo A, Ballesteros JJ, Schlosser L, Hernández-Vivanco A, Martín-Fernández M, Quintana R, Rayan A, et al. (2016). Activity-dependent switch of GABAergic inhibition into glutamatergic excitation in astrocyte-neuron networks. eLife 5, 10.7554/eLife.20362.

Petravicz J, Fiacco TA, and McCarthy KD (2008). Loss of IP3 receptor-dependent Ca2+ increases in hippocampal astrocytes does not affect baseline CA1 pyramidal neuron synaptic activity. J. Neurosci 28, 4967–4973. [PubMed: 18463250]

Saunders BT, Richard JM, Margolis EB, and Janak PH (2018). Dopamine neurons create Pavlovian conditioned stimuli with circuit-defined motivational properties. Nat. Neurosci 21, 1072–1083. [PubMed: 30038277]

Scofield MD, Boger HA, Smith RJ, Li H, Haydon PG, and Kalivas PW (2015). Gq-DREADD Selectively Initiates Glial Glutamate Release and Inhibits Cue-induced Cocaine Seeking. Biol. Psychiatry 78, 441–451. [PubMed: 25861696]

Serrano A, Haddjeri N, Lacaille JC, and Robitaille R (2006). GABAergic network activation of glial cells underlies hippocampal heterosynaptic depression. J. Neurosci 26, 5370–5382. [PubMed: 16707789]

Surmeier DJ, Bargas J, Hemmings HC Jr., Nairn AC, and Greengard P (1995). Modulation of calcium currents by a D1 dopaminergic protein kinase/phosphatase cascade in rat neostriatal neurons. Neuron 14, 385–397. [PubMed: 7531987]

Tang TS, and Bezprozvanny I (2004). Dopamine receptor-mediated Ca(2+) signaling in striatal medium spiny neurons. J. Biol. Chem 279, 42082–42094. [PubMed: 15292232]

Tritsch NX, and Sabatini BL (2012). Dopaminergic modulation of synaptic transmission in cortex and striatum. Neuron 76, 33–50. [PubMed: 23040805]

Uchigashima M, Narushima M, Fukaya M, Katona I, Kano M, and Watanabe M (2007). Subcellular arrangement of molecules for 2-arachidonoyl-glycerol-mediated retrograde signaling and its physiological contribution to synaptic modulation in the striatum. J. Neurosci 27, 3663–3676. [PubMed: 17409230]

Volterra A, and Meldolesi J (2005). Astrocytes, from brain glue to communication elements: the revolution continues. Nat. Rev. Neurosci. 6, 626–640. [PubMed: 16025096]

Volterra A, Liaudet N, and Savtchouk I (2014). Astrocyte Ca^{2+} signalling: an unexpected complexity. Nat. Rev. Neurosci 15, 327–335. [PubMed: 24739787]

Wang W, Dever D, Lowe J, Storey GP, Bhansali A, Eck EK, Nitulescu I, Weimer J, and Bamford NS (2012). Regulation of prefrontal excitatory neurotransmission by dopamine in the nucleus accumbens core. J. Physiol 590, 3743–3769. [PubMed: 22586226]

Zhang JM, Wang HK, Ye CQ, Ge W, Chen Y, Jiang ZL, Wu CP, Poo MM, and Duan S (2003). ATP released by astrocytes mediates glutamatergic activity-dependent heterosynaptic suppression. Neuron 40, 971–982. [PubMed: 14659095]

Zhang X, Zhou Z, Wang D, Li A, Yin Y, Gu X, Ding F, Zhen X, and Zhou J (2009). Activation of phosphatidylinositol-linked D1-like receptor modulates FGF-2 expression in astrocytes via IP3-dependent Ca2+ signaling. J. Neurosci 29, 7766–7775. [PubMed: 19535588]

Highlights

- Astrocytes in the Nucleus Accumbens respond to synaptic dopamine *in vivo*
- Astrocytes mediate the synaptic regulation induced by dopamine and amphetamine
- Amphetamine-induced enhancement in locomotion activity is modulated by astrocytes

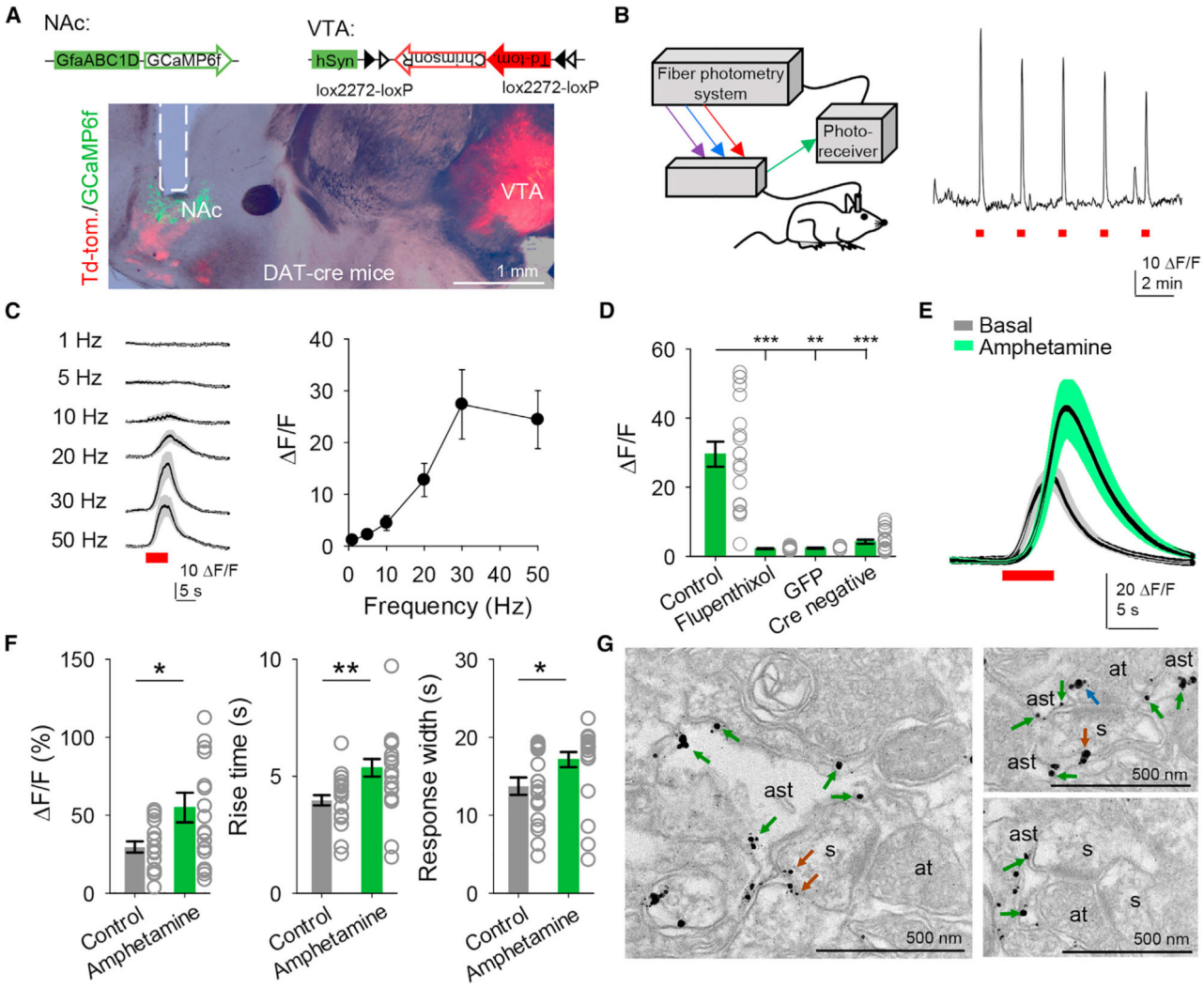

Figure 1. Astrocytes Respond to Dopamine *In Vivo*

A) Viral vectors used and image from DAT-Cre mice showing expression of ChrimsonR in the VTA and expression of GCaMP6f and the optic fiber track (dotted line) in the NAc. NAc, nucleus accumbens; VTA, ventral tegmental area.

(B) Scheme showing the fiber photometry system (left) and astrocyte responses to ChrimsonR activation (5 s, 30 Hz) in the NAc (right).

(C) Mean astrocyte responses to distinct stimulation frequencies.

(D) Mean fluorescence amplitude in response to ChrimsonR activation in the different experimental conditions (n = 19 stimuli from 5 animals for control, n = 14 stimuli from 2 animals for flupenthixol, n = 6 stimuli from 2 animals for GFP, and n = 23 stimuli from 4 animals for Cre negative). Kruskal-Wallis one-way ANOVA.

(E) Mean astrocyte responses to ChrimsonR activation before and after amphetamine administration.

(F) Mean fluorescence amplitude, response rise time, and width before and after amphetamine administration (n = 19 responses from 5 animals). Two-tailed Student's unpaired t test.

(G) Electron microscopy images showing D_1 receptors in astrocytes (green arrows), spines (brown arrows), and axon terminals (blue arrows). ast, astrocyte; s, spine; at, axon terminal. Data are expressed as mean ± SEM, *$p < 0.05$, **$p < 0.01$.

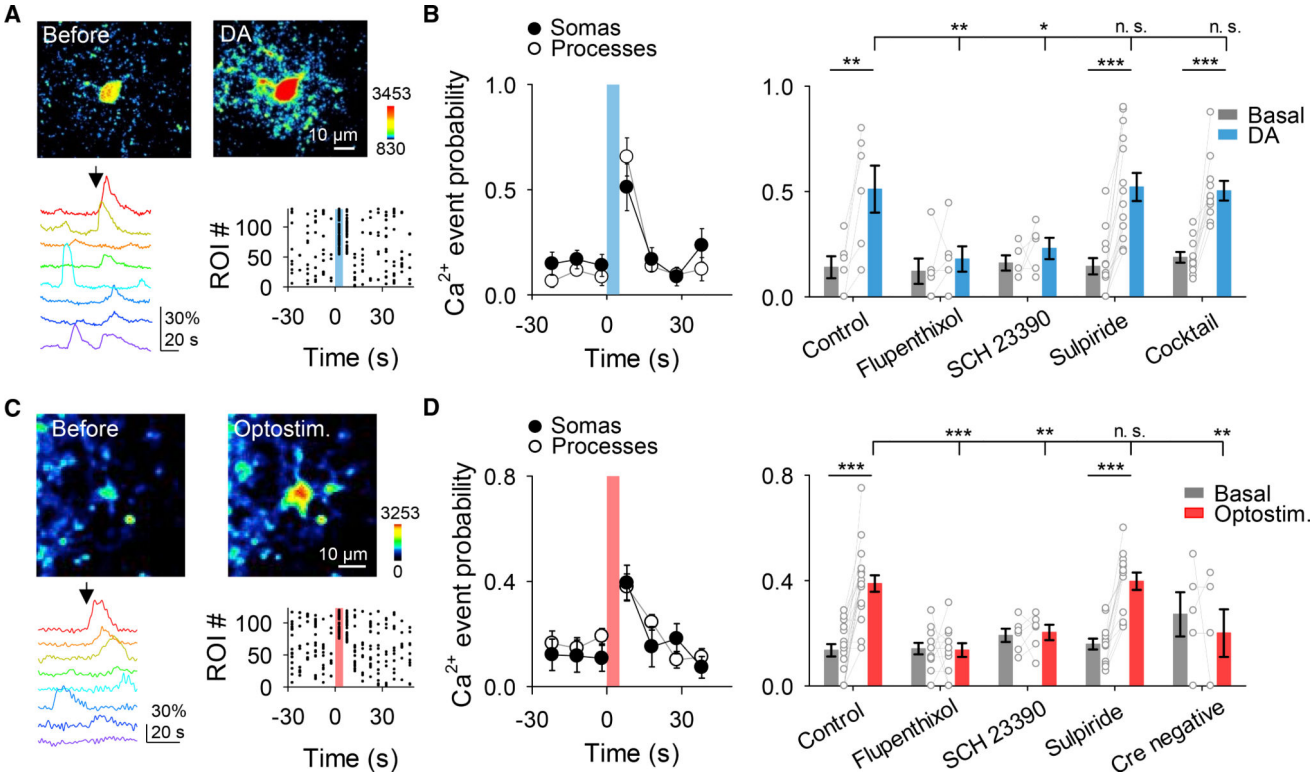

Figure 2. Astrocytes Respond to Dopamine through D_1 Receptors

A) Pseudocolor images showing the fluorescence intensities of GCaMP3-expressing astrocytes before and after dopamine (DA) application (top), representative Ca^{2+} traces of astrocytes (bottom left; arrow indicates DA application), and raster plot showing the Ca^{2+} events recorded from all ROIs including astrocyte somas and processes (bottom right). (B) Ca^{2+} event probability over time in somas and processes (left) and Ca^{2+} event probability before (basal) and after DA application in different experimental conditions (right). All experimental conditions were performed in TTX (1 μM). Cocktail of neurotransmitter receptor antagonists contained: CNQX (20 μM), AP5 (50 μM), MPEP (50 μM), LY367385 (100 μM), picrotoxin (50 μM), CGP5462 (1 μM), atropine (50 μM), CPT (10 μM), and suramin (100 μM). One-way ANOVA and two-tailed Student's paired t test. (C and D) Same as (A) and (B) but using opto-stimulation of dopaminergic axons instead of DA application. Experiments were performed in CNQX (20 μM), AP5 (50 μM), MPEP (50 mM), LY367385 (100 μM), picrotoxin (50 μM), CGP5462 (1 μM), atropine (50 μM), CPT (10 μM), and suramin (100 μM). One-way ANOVA and two-tailed Student's paired t test. Blue and red shadows indicate DA application and optical stimulation, respectively. Data are expressed as mean ± SEM, *$p < 0.05$, **$p < 0.01$, ***$p < 0.001$.

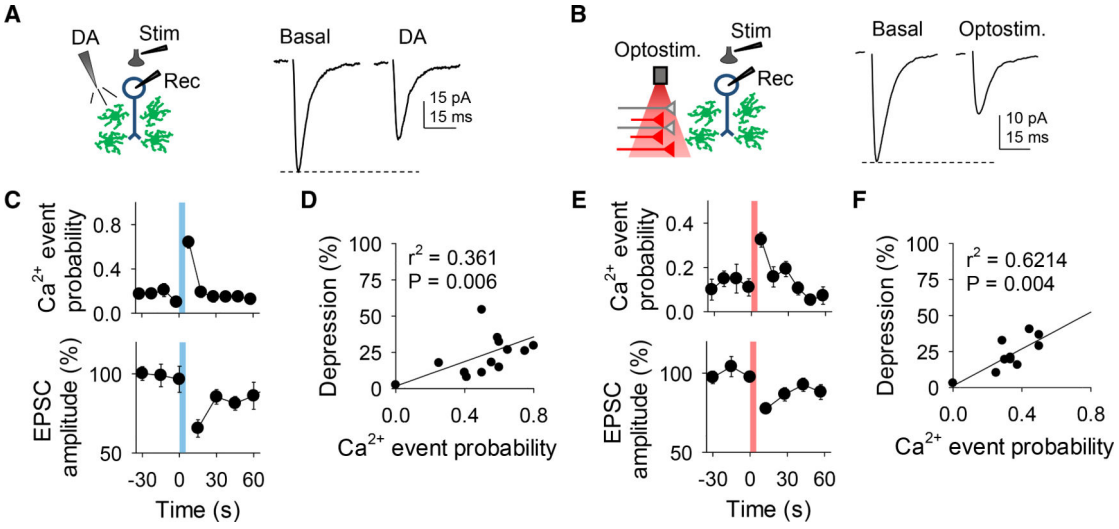

Figure 3. Dopamine Stimulates Astrocyte Ca^{2+} Increases and Neuronal Excitatory Transmission Depression

(A) Scheme of the experimental approach (left) and representative EPSC traces before (basal) and after DA application (right).

(B) As in (A) but for optical stimulation.

(C) Ca^{2+} event probability and relative EPSC amplitude over time.

(D) Relationship between Ca^{2+} event probability and change in EPSC amplitude after DA application.

(E and F) The same as (C) and (D) but for optical stimulation. Blue and red shadows indicate DA application and optical stimulation, respectively. Data are expressed as mean ± SEM.

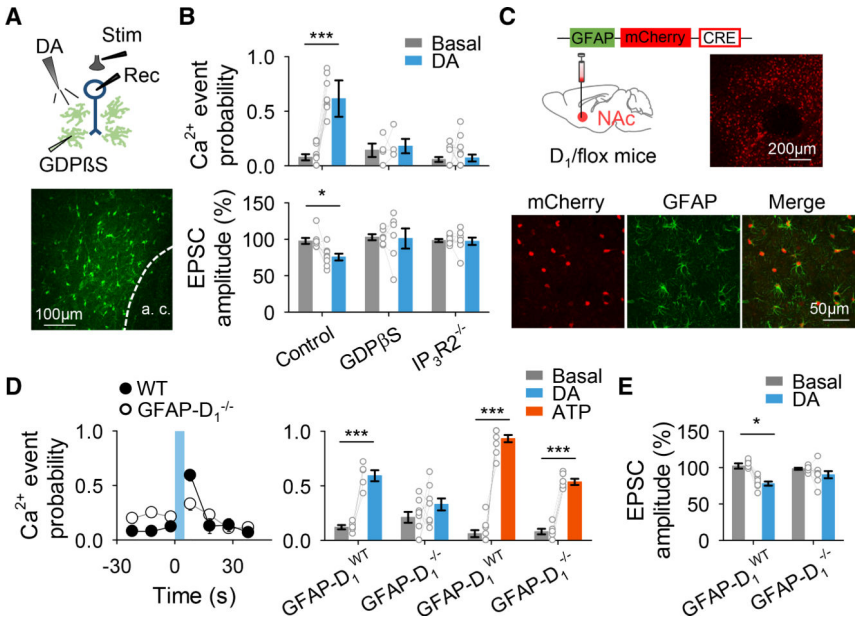

Figure 4. Astrocyte Ca^{2+} Is Necessary for DA-Evoked Synaptic Depression

(A) Scheme of the experimental approach (top) and fluorescence image of an astrocyte network loaded with biocytin through a patched astrocyte (bottom).

(B) Ca^{2+} event probability and relative EPSC amplitude before (basal) and after DA application. Two-tailed Student's paired t test.

(C) Viral vector injected into the NAc of D1-flox mice and fluorescence image showing mCherry-Cre expression in the NAc (top), and immunohisto-chemistry images showing co-localization between mCherry-cre and GFAP (bottom).

(D) Ca^{2+} event probability over time (left) and Ca^{2+} event probability before (basal) and after DA or ATP application (right). Blue shadow indicates DA application. Two-tailed Student's paired t test.

(E) Relative EPSC amplitude before (basal) and after DA application. Two-tailed Student's paired t test. Data are expressed as mean ± SEM, *p < 0.05, ***p < 0.001.

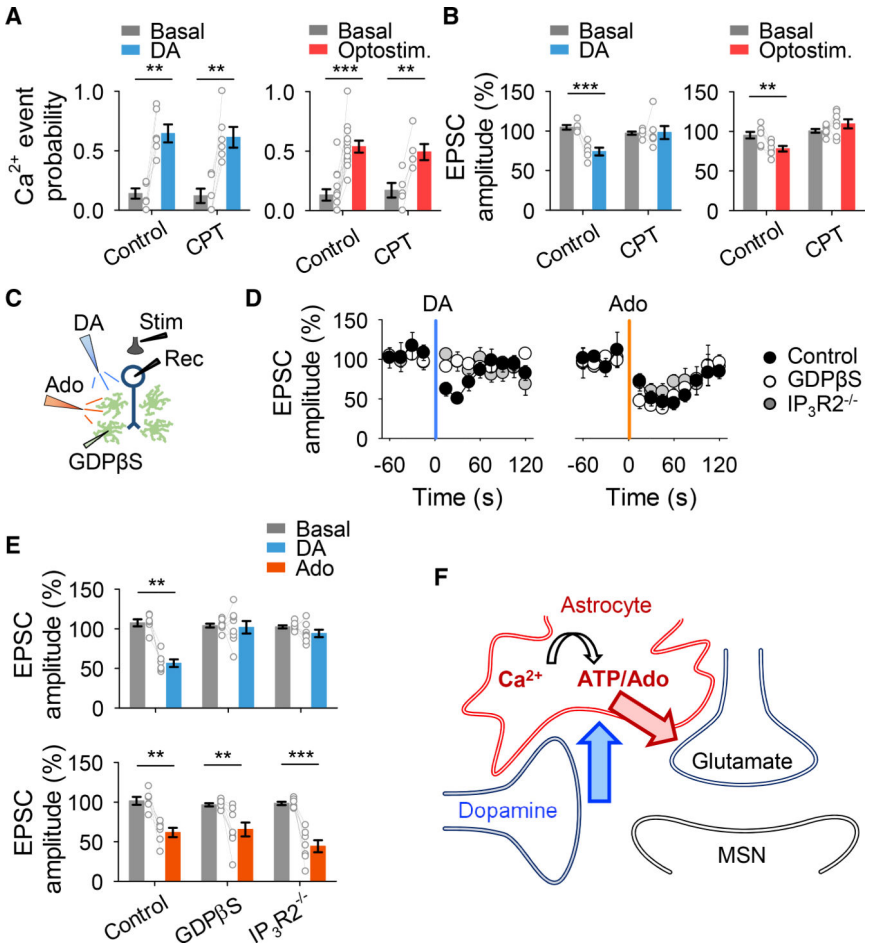

Figure 5. Astrocytes Mediate DA-Evoked Synaptic Depression via Adenosine Signaling

(A) Ca^{2+} event probability before (basal) and after DA application or opto-stimulation. Two-tailed Student's paired t test.

(B) Relative EPSC amplitude before (basal) and after DA application or opto-stimulation. Two-tailed Student's paired t test.

(C) Scheme of experimental approach.

(D) Relative EPSC amplitude over time. Blue and orange shadows indicate DA application and adenosine application, respectively.

(E) Relative EPSC amplitude before (basal) and after DA application or adenosine application. Two-tailed Student's paired t test.

(F) Schematic summary depicting the signaling pathways involved in DA-evoked synaptic depression. Data are expressed as mean ± SEM, **p < 0.01, ***p < 0.001.

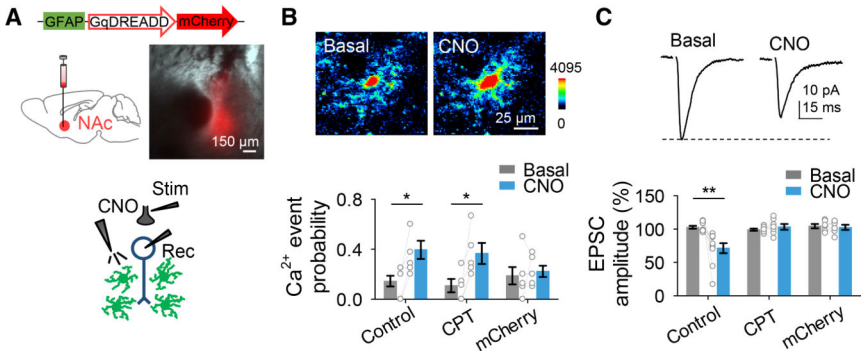

Figure 6. Astrocyte Ca^{2+} Is Sufficient for Excitatory Synaptic Depression

(A) Viral vector injected into the NAc and fluorescence image showing DREADD-mCherry expression in the NAc (top). Scheme of the experimental approach appears at bottom.

(B) Pseudocolor images showing the fluorescence intensities of GCaMP6f-expressing astrocytes before and after CNO application (top) and Ca^{2+} event probability before (basal) and after CNO application (bottom). Two-tailed Student's paired t test.

(C) Representative EPSC traces before (basal) and after CNO application (top) and relative EPSC amplitude before (basal) and after CNO application (bottom). Two-tailed Student's paired t test. Data are expressed as mean ± SEM, *p<0.05, **p< 0.01.

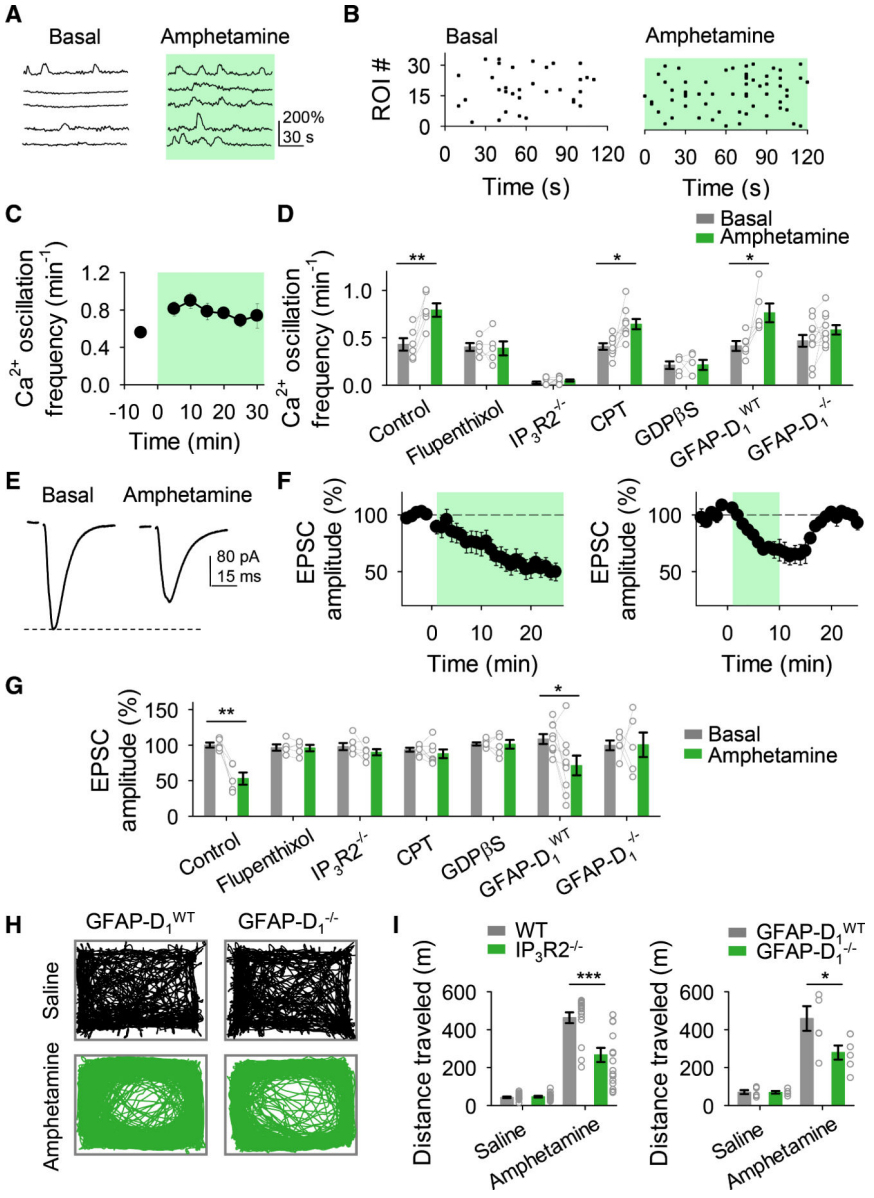

Figure 7. Astrocytes Are Involved in Amphetamine Synaptic Effects

(A) Representative Ca^{2+} traces of astrocytes in control (basal) and in the presence of amphetamine.

(B) Raster plots showing the Ca^{2+} events recorded from all ROIs including astrocyte somas and processes in control (basal) and in the presence of amphetamine.

(C) Ca^{2+} oscillation frequency over time.

(D) Ca^{2+} oscillation frequency in control (basal) and in the presence of amphetamine. Two-tailed Student's paired t test.

(E) Representative EPSC traces before (basal) and after amphetamine application.

(F) Relative EPSC amplitude over time.

(G) Relative EPSC amplitude before (basal) and in the presence of amphetamine. Two-tailed Student's paired t test.

(H) Representative traces of locomotor activity of mice injected with saline or amphetamine. (I) Distances traveled by different mice injected with saline or amphetamine (for $IP_3R2^{-/-}$ mice: n = 18; n = 8 males and n = 10 females; for $IP_3R2^{-/-}$ control wild-type mice: n = 16; n = 5 males and n = 11 females; for GFAP-$D_1^{-/-}$ mice: n = 6; n = 3 males and n = 3 females; for GFAP-D_1^{WT} mice: n = 6; n = 3 males and n = 3 females). Two-tailed Student's unpaired t test. Green shadow indicates amphetamine application. Data are expressed as mean ± SEM, *p < 0.05, **p < 0.01, ***p < 0.001.

KEY RESOURCES TABLE

REAGENT or RESOURCE	SOURCE	IDENTIFIER
Antibodies		
Mouse anti-NeuN	Millipore	Cat#: MAB377; RRID:AB_2298772
Rabbit anti-GFAP	Sigma	Cat#: G9269; RRID:AB_477035
Sheep anti-TH	Pel-Freez	P60101-0; RRID:AB_461070
Mouse anti-NG2	Millipore	Cat # 05-710; RRID:AB_309925
Rabbit anti-Iba1	Wako	Cat # 019-19741; RRID:AB_839504
Guinea pig anti-D1R polyclonal	Frontier Institute co., Japan	GP-Af500; C terminus 45 aa. of mouse D1R, NM010076; Cat# ATX-GP-Af500; RRID:AB_2721116
488 donkey anti-sheep	Molecular Probes	Cat# A-11015; RRID:AB_141362
405 goat anti-mouse	Molecular Probes	Cat# A-31553; RRID:AB_221604
488 goat anti-rabbit	Molecular Probes	Cat# A-11008; RRID:AB_143165
Goat anti-guinea pig IgG coupled to 1.4 nm gold	Nanoprobes Inc.	http://www.nanoprobes.com/products/FluoroNanogold.html
Bacterial and Virus Strains		
AAV8-GFAP-hM3D(Gq)-mCherry	UNC vector core	https://www.med.unc.edu/genetherapy/vectorcore/in-stock-aav-vectors/
AAV8-GFAP-mCherry	UMN vector core	http://vvcc.umn.edu/
AAV5-GfaABC1D-PI-LckGCaMP6.SV40	Penn Vector Core	https://gtp.med.upenn.edu/core-laboratories-public/vector-core
AAV5-GfaABC1D-cytoGCaMP6f-SV40	Penn Vector Core	https://gtp.med.upenn.edu/core-laboratories-public/vector-core
AAV8-GFAP-mCherry-CRE	UNC vector core	https://www.med.unc.edu/genetherapy/vectorcore/in-stock-aav-vectors/
AAV5-hSyn-FLEX-ChrimsonR-tdT	UNC vector core	https://www.med.unc.edu/genetherapy/vectorcore/in-stock-aav-vectors/
Experimental Models: Organisms/Strains		
C57BL/6J	The Jackson Laboratory	JAX #000664
$IP_3R2^{-/-}$	Li et al. (2005)	N/A
DrD1 flox/flox	The Jackson Laboratory	JAX #025700
DAT-IRES-CRE	The Jackson Laboratory	JAX #006660
R26-lsl-GCaMP3 mice	The Jackson Laboratory	JAX #014538
GLAST-CreERT2	The Jackson Laboratory	JAX #012586
Software and Algorithms		
Clampfit 10.4	Molecular Devices	https://www.moleculardevices.com/
MetaMorph 7.8.8.0	Molecular Devices	https://www.moleculardevices.com/
Fluoview	Olympus	https://www.olympus-lifescience.com/en/

REAGENT or RESOURCE	SOURCE	IDENTIFIER
LAS AF Lite	Leica	https://www.leica-microsystems.com/
RZ5P processor	Tucker Davis Technologies	https://www.tdt.com/component/fiber-photometry-rz5p/
ANY-maze	Stoelting Co.	https://www.stoeltingco.com/anymaze.html?gclid=EAIaIQobChMI8avNqv7p5AIViLzACh1YBgfLEAAYASAAEgI3OfD_BwE
SigmaPlot 12.5	Systat Software Inc.	https://systatsoftware.com/products/sigmaplot/sigmaplot-product-updates/
ImageJ	NIH	https://imagej.nih.gov/ij/
MATLAB	MathWorks	https://www.mathworks.com/products/matlab.html